Available online at www.sciencedirect.com

ScienceDirect

Advances in Space Research 74 (2024) 1497–1517

ADVANCES IN SPACE RESEARCH (a COSPAR publication)

www.elsevier.com/locate/asr

Extracting very small amounts of potassium from iron meteorites for the analysis of potassium isotope ratios

H. Khan [a], I. Leya [a,*], J. Hoffmann [b], K. Mezger [b]

[a] Space Science and Planetology, Physics Institute, University of Bern, Switzerland
[b] Institut für Geologie, University of Bern, Switzerland

Received 31 October 2023; received in revised form 26 March 2024; accepted 5 May 2024
Available online 10 May 2024

Abstract

The isotope abundance of cosmogenic K, especially the ratios of cosmogenic $^{40}K/^{41}K$, can be used to determine reliable cosmic-ray exposure (CRE) ages for iron meteorites. Despite this potential, there are only very few studies and essentially no new data since the pioneering work by H. Voshage more than 40 years ago. This shortfall is likely due to the immense analytical difficulties encountered when extracting cosmogenic K from iron meteorites with typical concentrations in the range of a few ppb or below. Chemical extraction procedures are very challenging, resulting in large blank contributions that must be subtracted, and do have low yields preventing an efficient separation of K from the Fe matrix. The K extracted from iron meteorites is dominated by native K (non-cosmogenic K from the sample), includes K from terrestrial contamination, and only a tiny amount is of cosmogenic origin. In order to separate K from iron meteorites a physical extraction technique was developed that involves extraction of K from molten iron meteorites. In this set-up, terrestrial and native K can be partly separated from cosmogenic K by sophisticated pre-heating and extraction techniques. Sample K is ion-optically collected on a rhenium filament. The filaments are then used as evaporation filaments in a double filament set-up of a Triton Plus Thermal-Ionization Mass Spectrometer (TIMS). Though, cosmogenic K is detectable in all samples, the measured isotope ratios are always close to terrestrial, indicating that the majority of the measured ^{39}K and ^{41}K is from K with almost terrestrial isotope composition. The measured ^{40}K signal is dominantly of cosmogenic origin. The K background is either native K from the sample or terrestrial contamination. The measurements are compromised by unstable signals, i.e., by large fluctuations of the ion currents and/or large variations in the isotope ratios during the course of a single run, sometimes even with fractionation reversals. Such difficulties are likely due to the fact that the K ions are implanted into the filament rather than deposited onto the surface. In addition, parts of the filaments are covered with condensed iron, also affecting the signal stability. Despite these analytical challenges, clear cosmogenic signals were detected in almost all studied iron meteorites and cosmogenic $^{40}K/^{41}K$ ratios could be determined. However, the data quality is not yet sufficient for precise K isotope studies and for calculating reliable $^{40}K/^{41}K$ CRE ages for iron meteorites.

Keywords: Cosmogenic Nuclides; Cosmic Rays; Iron Meteorites; Cosmic Ray Variations

1. Introduction

The ^{40}K-K dating system for cosmic-ray exposure (CRE) ages is based on the fact that the concentrations of the two stable cosmogenic, i.e., produced by cosmic-rays, nuclides ^{39}K and ^{41}K linearly increase with cosmic-ray exposure time. In contrast, the concentration of cosmogenic ^{40}K, which is radioactive with a half-live

* Corresponding author.
E-mail addresses: hmk_khan@hotmail.com (H. Khan), Ingo.Leya@unibe.ch (I. Leya), Jan.Hoffmann@unibe.ch (J. Hoffmann), Klaus.Mezger@unibe.ch (K. Mezger).

https://doi.org/10.1016/j.asr.2024.05.006
0273-1177/

of 1.248 × 10^9 years (Kossert and Günther, 2004), increases exponentially. For very long exposure times (not reached in meteorites), ^{40}K reaches saturation, i.e., radioactive decay and production become equal and the concentration of cosmogenic ^{40}K becomes time-independent. Due to this exponential increase, the ^{40}K concentration always increases slower than the ^{39}K and ^{41}K concentrations, which permits determining CRE ages. CRE ages derived with the ^{40}K-K system are important data for a variety of applications, ranging from astrophysics to climatology. For example, whether the fluence of galactic cosmic rays (GCR) inside but also outside the solar system was constant over long time periods is one of the most important questions in planetary sciences and astrophysics. A constant GCR flux is usually implied for the interpretation of CRE age histograms, which are powerful tools when studying the collisional history of small solar system bodies like asteroids, meteoroids, and micrometeoroids.

In a series of papers Shaviv (2002, 2003) and Scherer et al. (2006) argued that cosmogenic nuclides in iron meteorites provide evidence for periodic variations of the GCR fluxes, caused by the periodic passage of the solar system through galactic spiral arms. In spiral arms, star formation and supernova rates are higher, leading to an increased GCR flux. The presumed periodicity of the GCR flux has also been linked to the occurrence of ice age epochs on Earth via more extensive global cloud coverage during times of higher GCR intensity (Shaviv, 2003; Shaviv and Veizer, 2003). Although some studies were supportive (e.g., Wallmann, 2004; Gies & Helsel, 2005), many subsequent investigations have questioned the original hypothesis (e.g., Sloan and Wolfendale, 2013) and/or re-interpreted the iron meteorite data and either found no indications for a periodicity (Rahmstorf et al., 2004; Jahnke, 2005; Wieler et al., 2013) or indications for a periodicity but with a different period (Alexeev, 2016). In summary, Wieler et al. (2013) concluded that the known exposure ages for iron meteorite are too uncertain to detect GCR flux variations smaller than a factor of about two.

In addition to periodic GCR intensity variations there are also indications for a one-time and sudden increase in the GCR intensity with a higher flux in the past several Ma, relative to the long-term average over the past 500–1000 Ma (e.g., Hampel and Schaeffer, 1979; Aylmer et al., 1988; Lavielle et al., 1999; Wieler et al., 2013). In all these studies, the CRE ages calculated via ^{10}Be-^{21}Ne, ^{26}Al-^{21}Ne, and/or ^{36}Cl-^{36}Ar were compared to ^{40}K-K CRE ages determined earlier by H. Voshage (e.g., Voshage and Hintenberger, 1959,1961; Voshage, 1967,1978,1984; Voshage and Feldmann, 1979; Voshage et al., 1983). As an example, Smith et al. (2019) measured ^{36}Cl-^{36}Ar CRE ages for 57 iron meteorites, 43 of them being from the largest group IIIAB, and found no indications for periodic GCR variations. In the same study, the authors also tested the database for indications of a one-time sudden change in GCR intensity by comparing ^{36}Cl-^{36}Ar CRE ages to ^{40}K-K CRE ages measured earlier by H. Voshage (e.g., Voshage, 1984). The data indicate that the GCR intensity in the time interval 95–656 Ma (Ma: Mega-annum, time before present) might have been up to 40 % lower than the GCR intensity over the last few Ma (Smith et al., 2019). Since such a large change seems unrealistic, the authors concluded that there is likely a systematic bias between the ^{36}Cl-^{36}Ar and ^{40}K-K dating systems. However, this conclusion is not very robust, because the comparison between ^{36}Cl-^{36}Ar and ^{40}K-K ages is based only on 11 meteorites due to the lack of ^{40}K-K ages, which clearly demonstrates the need to determine more ^{40}K-K CRE ages.

While ^{40}K-K ages are commonly used for such studies, they are not without problems. The production of cosmogenic ^{39}K, ^{40}K, and ^{41}K in iron meteorites is poorly studied and depends on radius and shielding of the body. It is also possible, but has never been tested, that the ^{39,40,41}K production rates and production rate ratios depend on the Fe/Ni ratio of the meteorite. Production rates are needed for CRE age studies, but because they are not known, the original studies used relationships between ^{39}K/^{41}K and ^{4}He/^{21}Ne ratios (e.g., Voshage, 1967; Voshage and Feldmann, 1979; Voshage, 1978,1984; Voshage et al., 1983). However, Ammon et al. (2008a) argued that this relationship is most likely compromised by too high and variable cosmogenic ^{21}Ne concentrations caused by contributions from the abundant trace elements S and P. Such likely variable contributions are not accounted for in the empirical relationship. Consequently, the relationship used in the original studies on which all ^{40}K-K ages and therefore all further studied are based, is most likely not as reliable as it needs to be for precise CRE age determinations.

Furthermore, the existing ^{40}K-K database covers only meteorites analyzed before 1984 (e.g., Voshage, 1984), i.e., there are no new data for 40 years although the meteorite collections grew significantly since then. Finally, the database only covers meteorites with CRE ages older than 100 Ma, which was the lower limit for obtaining precise ages (e.g., Voshage, 1967; Voshage and Feldmann, 1979; Voshage, 1978,1984; Voshage et al., 1983). Consequently, there is an urgent need to re-evaluate the existing ^{40}K-K ages, to reduce their uncertainties, and especially to obtain new data.

Despite the importance and potential of ^{40}K-K ages, there was only little effort to re-establish the K extraction system and to extend and improve the database. The major challenge in any study of cosmogenic K is the low concentration, which is at a level of 10^{-9} g/g. This small amount must be separated from the overwhelming amounts of native K, which commonly is at a level of 10^{-6} g/g in iron meteorites, i.e., three orders of magnitude higher than the cosmogenic K concentration. Native K either resides along grain boundaries, in troilite inclusions, or simply stems from terrestrial contamination.

Wet-chemical extraction techniques cannot easily distinguish between native K, contamination, and cosmogenic K and therefore suffer from a high background of non-

cosmogenic K. Despite the problems, there were some relatively successful K isotope studies using chemical extraction. Imamura et al. (1980) studied the spallogenic production of K, Ca, Ti, V, and Mn in iron meteorites. They were able to determine cosmogenic ^{40}K concentrations in 12 samples from the iron meteorite Grant and in 6 samples from the iron meteorite Treysa with an accuracy in the range of 2–4 %. However, they had to conclude that the cosmogenic ^{40}K/^{41}K ratios are too uncertain for the determination of CRE ages. For example, the multiple measurements of the meteorite Grant showed a total K concentration in the range of 100–470 ppb, of which only ~ 1 ppb was of cosmogenic origin. Later Birck and co-authors studied the iron meteorites Grant and Carbo (e.g., Birck and Allegre, 1983,1985). However, their focus was on the production systematics of Li, Mg, K, Ca, Ti, V, and Cr and not on the determination of CRE ages. More recently, Shankar (2011) tried with limited success measuring K isotope ratios in iron meteorites with the aim of re-calculating CRE ages. For this study, K was chemically extracted from seven iron meteorites (Brownfield, Charlotte, Carbo, Grant, Picacho, Signal Mountain, Treysa) and the K isotope ratios were measured in two of them (Brownfield, Picacho). The age of 378 Ma (no uncertainties are given in this study) for Brownfield agrees with the age of 355 ± 70 Ma given by Voshage and Feldmann (1979). Smith et al. (2019) used the ^{36}Cl-^{36}Ar dating system and determined a CRE age of 243 ± 18 Ma for this meteorite. For the iron meteorite Picacho, Shankar (2011) determined a CRE age of 190 Ma (without an uncertainty), which is substantially shorter than the CRE age of 635 ± 55 Ma given by Voshage and Feldmann (1979). The age of 432 ± 32 Ma obtained by Smith et al. (2019) is in-between the two, but is closer to the age determined by Voshage and Feldmann (1979). The problems and challenges in the study by Shankar (2011) were the high blanks in some analyses and the poor reproducibility of yields after the chemical extraction procedure. The advantage of the wet chemical extractions is that all K components (cosmogenic, native, contamination) are extracted together and the sample can be loaded evenly on a filament allowing for stable signals and high precision isotope ratio measurements. In addition, a ^{39}K spike can be added to estimate the amount of terrestrial contamination and/or native K (Imamura et al., 1980).

The physical extraction system, which was pioneered by Voshage and Hintenberger (1959, 1961) and Voshage (1967), is superior for separating small amounts of cosmogenic K from the overwhelming amount of native K, because it enables a preheating step at a temperature slightly lower than the melting temperature of iron meteorites, in which K from the surface but also from grain boundaries is evaporated, while cosmogenic K still remains in the sample. Upon further heating, K from the sample is trapped/implanted into a filament that is later measured using thermal ionization mass spectrometry. The disadvantage is that only a small amount of the K is collected on the filament and this is often partly covered with condensed iron. This makes the sample difficult to measure, as neither the signals nor the fractionation of the isotope ratios are constant for such a sample. Consequently, data processing must be very sophisticated.

In summary, the major challenge measuring cosmogenic K isotopes in iron meteorites are the extremely low concentrations. For example, Imamura et al. (1980) reported for the iron meteorites Grant and Carbo cosmogenic ^{40}K concentrations of 0.30–0.36 ppb and 0.39–0.43 ppb, respectively. Similarly low concentrations were found by Shankar (2011) for Brownfield (0.96 ppb) and Picacho (0.52 ppb). At the same time, concentrations of native K and of K from terrestrial contamination in iron meteorites are often significantly higher than the cosmogenic K concentrations (e.g., Voshage and Hintenberger, 1959), requiring an efficient and highly selective extraction method.

The present study presents the basics of the physical extraction system recently developed and constructed at the University of Bern with the goal to establish a method to reliably and reproducibly extract K from iron meteorites, to efficiently separate cosmogenic K from native and terrestrial K, to determine the cosmogenic ^{40}K/^{41}K isotope ratios, and finally to calculate CRE ages (see also Khan, 2022). In addition, it highlights some of the problems and specialties of the TIMS measurements owing to the fact that the sample is implanted into the filament rather than deposited on its surface.

2. Experimental methods – Potassium extraction

2.1. Basics of the physical extraction procedure

The physical extraction technique for K from iron meteorites is based on the principles of fractional evaporation. Potassium is more volatile than Fe; the evaporation temperature for K is 760 °C and the melting temperature for Fe is 1535 °C. Therefore, K can evaporate from an iron melt. In addition, K has a low first ionization potential of only 4.34 eV and a low electronegativity of 0.82 on the dimensionless Pauli scale. Since the electronegativity of Fe is much higher (1.83), the electron from the K can be part of the electron cloud of the Fe metal, leaving the K ionized. By applying a sufficiently high electric field, the positive K ions can be extracted, collected, and concentrated onto filaments and/or samples holders using ion-optical procedures. The basic set-up of our extraction system is related to the instrument originally developed by H. Voshage (e.g., Voshage and Hintenberger, 1959,1961; Voshage, 1967,1978,1984).

There are (at least) three important aspects that must be evaluated before reliable data can be produced. First, are there any significant fractionation effects during the entire sample extraction procedure? Second, are there any significant effects caused by implantation of K into the filament instead of it being deposited on the filament surface? Third,

how much Fe is condensing onto the filament, which likely controls the signal intensity and stability during TIMS measurements? Mass fractionation is discussed below, ion implantation and Fe evaporation/condensation is discussed in Appendix 1 and 2, respectively.

The basic set-up of the K extraction system is shown in Fig. 1 and a more detailed engineering drawing is shown in Fig. 2. It is a high vacuum system consisting of an upper (inner) and a lower (outer) part, separated by the crucible. The lower part contains the RF coil used for heating the crucible, which both are inside the lower vacuum part to protect the outer part of the crucible from oxidation and damage during heating. An RF generator (Linn High Therm®, Germany) is used for heating with its coils inside the vacuum chamber. The construction requires feedthroughs able to withstand the high frequencies and currents needed for RF heating, but at the same time permit the necessary water cooling of the coil. In the designed RF-set-up, all RF-connections are kept below 400 °C, i.e., below the upper temperature limit for feedthroughs and gaskets. In order to increase the heating efficiency and to minimize heating damage *inside* the system, an assemblage of tantalum foils serves as a heat shield. In this set-up, the crucible can be heated up to ~ 1800 °C and the outside of the vacuum system never exceeds ~ 150 °C, a temperature far lower than the critical temperature for the copper gaskets and the feedthroughs. Some details of the extraction procedure are given in Appendix 3. During the project, the system underwent some significant changes, which are summarized in Appendix 4.

2.2. Mass-dependent isotope fractionation and mixing of K isotopes

The extraction procedure for K from the metal matrix involves fractional evaporation followed by ion-optical extraction, and subsequent collection on or in a rhenium filament. Due to the strong electric field applied between sample and filament, large mass-dependent fractionation effects due to incomplete K collection are not expected. Assuming the exponential fractionation law, which is commonly used in mass spectrometry (Dauphas and Schauble, 2016), the fractionated ratio is related to the "true" unfractionated ratio via:

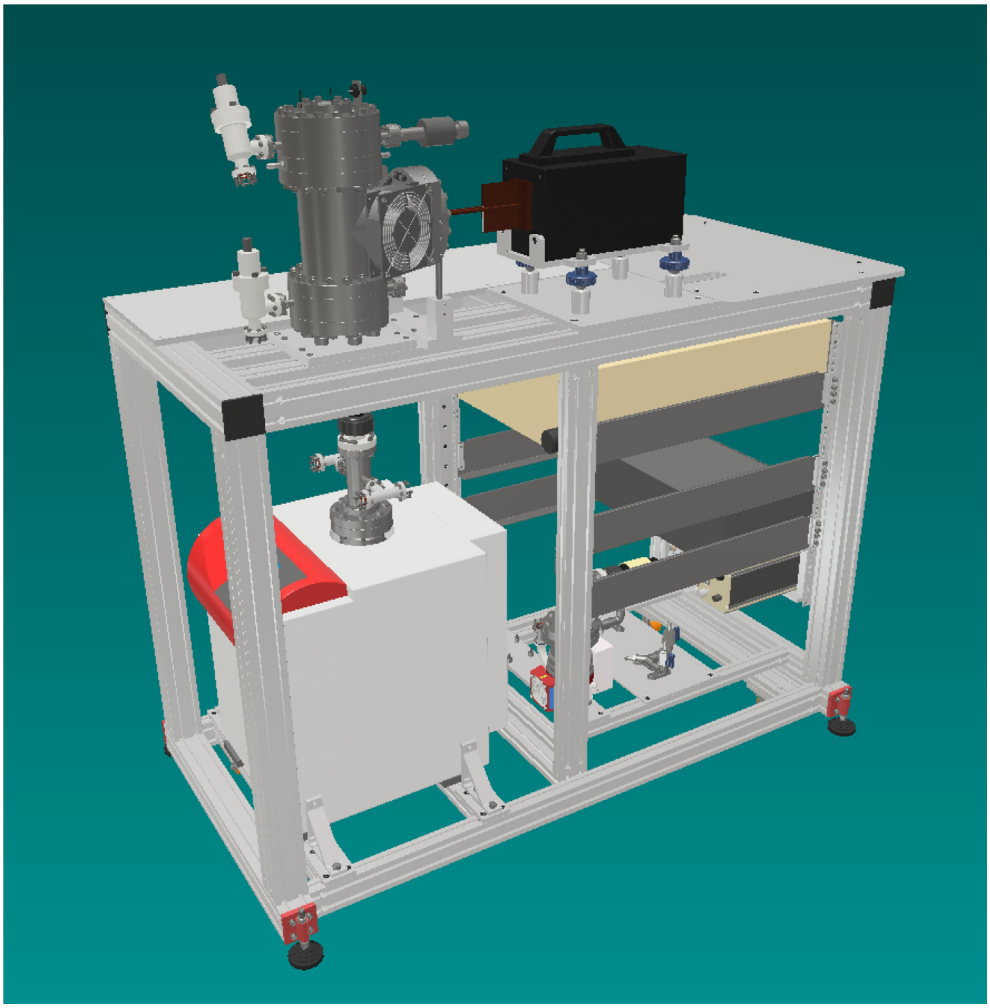

Fig. 1. View of the K extraction system constructed and installed at the University of Bern. The dimensions are: total height = 1380 mm, total length = 1340 mm, and total width = 650 mm.

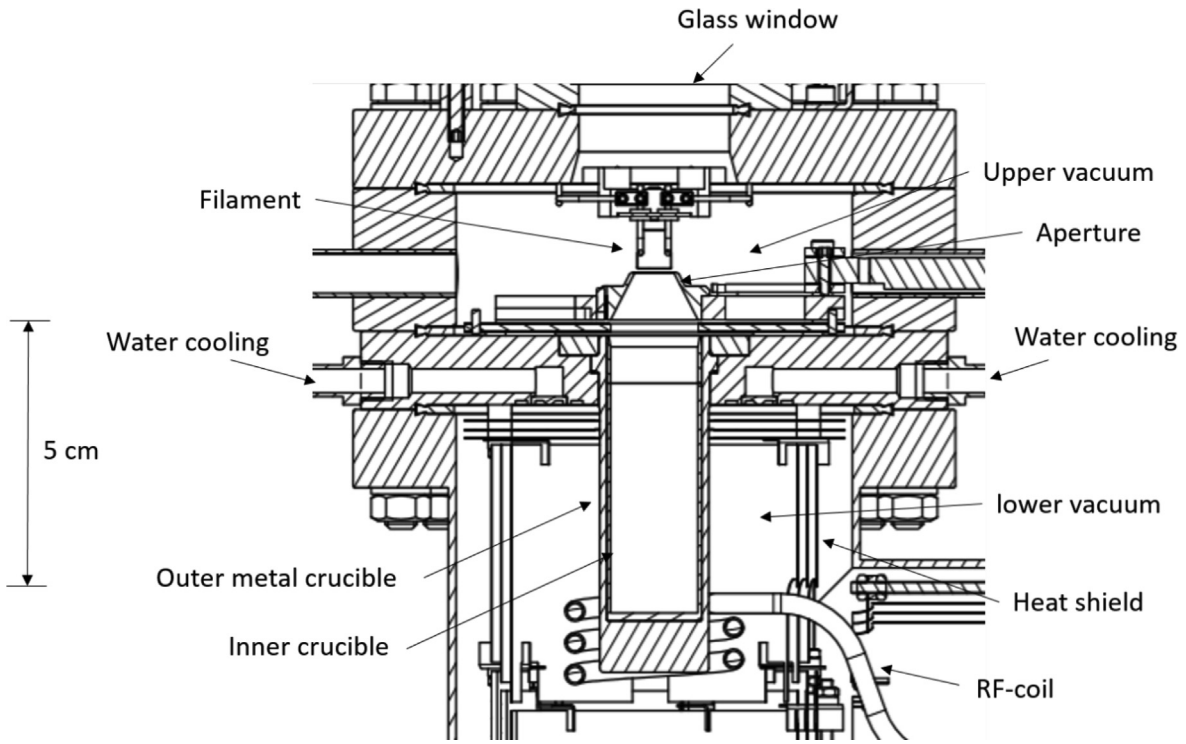

Fig. 2. Engineering drawing of the K extraction system. The upper part comprises the inner part of the crucible, the aperture above the crucible, and the filament. The lower parts consist of the RF heating coil and the heat shields. The RF coil and the flange holding the crucible are both water cooled. The vacuum in the two parts of the extraction system is separated by the crucible.

$$\left(\frac{iK}{39K}\right)_{fractionated} = \left(\frac{iK}{39K}\right)_{true} \times \left(\frac{m_i}{m_{39}}\right)^{\beta} \quad (1)$$

with i either 40 or 41, depending on the ratio, m_i the atomic masses and β a free parameter. In "normal" isotope studies, β is determined by measuring standards with known isotope ratios and comparing the measured ratios to the true ratios (also using equation 1). Unfortunately, having appropriate standards is almost impossible for the present study (see below). By using the terrestrial ratios as the "true" values and varying β, the mass dependent fractionation (*mdf*) line can be calculated. In a diagram $^{40}K/^{39}K$ as a function of $^{41}K/^{39}K$, the *mdf* line has a slope 8.3×10^{-4} (Fig. 3). In addition to the terrestrial ratio (open dot) and the *mdf*-line, Fig. 3 also shows estimates for cosmogenic K (Voshage, 1967) and the mixing line between native and cosmogenic K. The numbers shown along the mixing line stand for the ratios of native K relative to cosmogenic K (using the total number of K atoms). Considering the absolute ratios, there is a clear distinction between the *mdf*-line and the cosmogenic ratios, which allows distinguishing whether the measured data indicate fractionated terrestrial ratios or contributions from cosmogenic K.

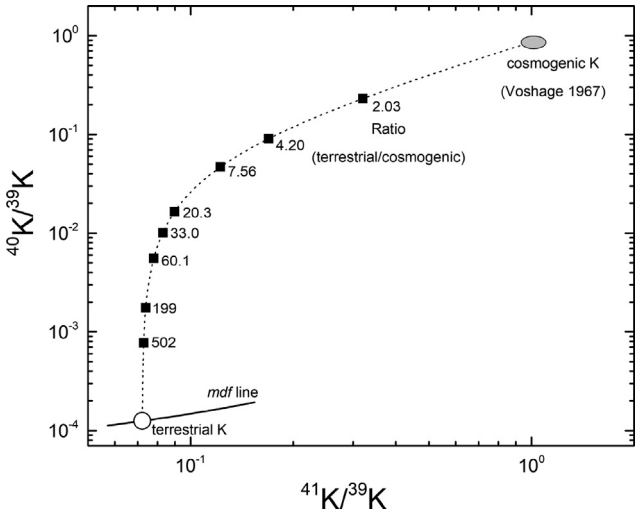

Fig. 3. Fractionation and mixing pattern of the K isotope composition expected in iron meteorites. Native K from the sample and terrestrial contamination is expected to have terrestrial isotope composition. The mass-dependent fractionation line is plotted through the terrestrial isotope composition. The mdf line can be moved upwards or downwards depending on the initial K isotope composition. The slope $\sim 8.3 \times 10^{-4}$, however, remains unchanged. Also shown is the expected composition of cosmogenic K (Voshage, 1967) and the mixing line between cosmogenic and native K. The numbers along the mixing line give the ratio of native K relative to cosmogenic K (in total number or atoms).

3. Experimental methods – TIMS measurements

3.1. Interpretation of the TIMS data

Due to the sometimes large variations of the individual ion currents during a TIMS measurement for some of the samples, the data handling procedure had to be adjusted. In a regular TIMS set-up, the isotope ratios are calculated by averaging individual ratios obtained from individual

measurement cycles. For a sample, the final $^{41}K/^{39}K$ ratio is then given as the average of the $^{41}K/^{39}K$ ratios obtained from hundreds to thousands of individual measurement cycles. In this study a method very similar to the "total evaporation method" was used instead. All individual readings for the individual K isotopes, i.e., voltages for ^{39}K and ^{41}K and counts for ^{40}K, were added up and the $^{41}K/^{39}K$ and $^{40}K/^{39}K$ ratios were calculated from the integrated signals. With this procedure, ratios measured at low ion intensity have less weight than ratios measured at high ion intensity. Thus calculated ratios are much more representative for the entire sample. As a disadvantage of this procedure, calculating uncertainties is no longer straightforward. For the normal total evaporation method, one usually determines the precision of the method by repeatedly measuring the total evaporation of a set of *N* aliquots. From such *N* repeated measurements, the standard deviation can then be calculated. For references see, e.g., Ogliore et al. (2011) and Coath et al. (2013). In this initiating phase, however, which aims to demonstrate the procedure, no such systematic study was performed.

The K isotope ratios for the samples are expected to be a mixture between terrestrial K ($^{40}K/^{39}K = 0.000125116$ and $^{41}K/^{39}K = 0.0721677$, e.g., Naumenko et al., 2013) and cosmogenic K with isotope ratios in the range $^{41}K/^{39}K = 0.969 - 1.038$ and $^{40}K/^{39}K = 0.85 - 0.88$ (Voshage, 1967). Because of this mixture, measured K isotope ratios cannot be corrected for instrumental mass fractionation. First, the data cannot be internally normalized because neither $^{40}K/^{39}K$ nor $^{41}K/^{39}K$ are normal and can be used as a reference. Second, the standard-sample bracketing method cannot be applied because our standards are not a good match for the sample (loaded onto the filament vs. implanted into the filament). In addition, to our knowledge, there exist no metal standard with a known, homogeneous (on a gram level), and low (in the range of 100 ppb) K concentration. The uncorrected data are presented in a diagram $^{40}K/^{39}K$ vs. $^{41}K/^{39}K$ (e.g., Fig. 3). In such a diagram, terrestrial K, i.e., standards and terrestrial contamination, but also native K from the sample, plot to the lower left and cosmogenic K to the upper right. Fig. 3 also shows the line for mass-dependent fractionation (*mdf*-line). Mass-dependent fractionation on the filament during analysis leads to the detection of initially light isotope ratios (low $^{40}K/^{39}K$ and $^{41}K/^{39}K$) that gradually grow heavier (high $^{40}K/^{39}K$ and $^{41}K/^{39}K$) as the measurement progresses and the sample amount on the filament decreases. The isotope ratios detected throughout a measurement move approximately along the modelled *mdf*-line. In contrast, cosmogenic contributions move the ratios towards higher values but not along the *mdf*-line. As discussed in Appendix 2; the implantation process is not expected to significantly fractionate K isotopes, because the implantation depths for all three isotopes are very similar. Even though the sample data are not corrected for mass fractionation, mass fractionation factors are nevertheless discussed for the standards measured in combination with the samples to demonstrate a low and relatively constant fractionation, which demonstrates the reliability of the TIMS set-up.

In the first step of data treatment, all cycles with readings close to the baseline, i.e., below 1 mV for one of the K isotopes (usually the least-abundant ^{40}K if measured on a Faraday Cup), were considered unreliable and not considered further. For some samples and for all standards, the ion currents were relatively constant and a normal data handling procedure based on averaging individual ratios was used. However, before calculating average ratios an outlier test was performed. *First*, the 1st and 3rd quartiles and the interquartile range iqr = 3rd quartile – 1st quartile were calculated. Next, the upper boundary and the lower boundary were calculated via upper = 3rd quartile + (1.5 × iqr) and lower boundary via lower = 1st quartile – (1.5 × iqr). All data above or below the upper and lower boundary, respectively, were rejected. For most runs there were very few rejections. The average ratios were then calculated from the remaining data. The thus calculated averages and their 2σ uncertainties are given in Table 1 for the standards and Tables 4 and 5 for the samples. Data calculated this way for the samples are labelled "normal averages".

In addition, all data, i.e., all individual ratios obtained from hundreds to thousands of measurement cycles, are shown in $^{40}K/^{39}K$ vs. $^{41}K/^{39}K$ diagrams. This enables the use of the same data but interpreting them in slightly different ways. Some of the data plot on a linear array connecting the terrestrial ratio with cosmogenic K. In such a case, the slope of the correlation line, if forced through the data

Table 1
$^{40}K/^{39}K$ and $^{41}K/^{39}K$ ratios measured for terrestrial standards with 100 ng, 50 ng, 25 ng, 5 ng, and 1 ng of K on the filament.

K amount on filament (ng)	$^{40}K/^{39}K$ [10^{-4}]	$^{41}K/^{39}K$ [10^{-2}]
100	1.24011 ± 0.00597	7.20483 ± 0.00844
100	1.23674 ± 0.00544	7.19462 ± 0.00267
100	1.23838 ± 0.00485	7.20484 ± 0.00820
100	1.24015 ± 0.00496	7.20255 ± 0.00381
Average 100 ng	**1.23883 ± 0.00262**	**7.19816 ± 0.00205**
50	1.23980 ± 0.00449	7.20311 ± 0.00234
50	1.24032 ± 0.00456	7.20420 ± 0.00805
50	1.24113 ± 0.00377	7.19759 ± 0.00863
50	1.24024 ± 0.01270	7.20457 ± 0.00788
Average 50 ng	**1.24050 ± 0.00240**	**7.20296 ± 0.00210**
25	1.24059 ± 0.00453	7.20791 ± 0.00477
25	1.24269 ± 0.00498	7.21667 ± 0.00601
25	–	7.20411 ± 0.01140
Average 25 ng	**1.24154 ± 0.00335**	**7.21060 ± 0.00355**
5	1.23654 ± 0.00875	7.22433 ± 0.01631
5	1.24233 ± 0.03257	7.23422 ± 0.12687
5	1.23846 ± 0.00656	7.22706 ± 0.01839
5	1.23837 ± 0.01081	7.22867 ± 0.01646
Average 5 ng	**1.23795 ± 0.00407**	**7.22669 ± 0.00097**
1	–	7.20211 ± 0.17338
1	–	7.22289 ± 0.00208
1	–	7.07337 ± 0.45933
1	–	7.15833 ± 0.52779
Average 1 ng	–	**7.22288 ± 0.00208**

for the standards, gives the $(^{40}K/^{41}K)_{cos}$ ratio of the sample, which is the data relevant for calculating CRE ages.

There is a third way of interpreting some of the data. Since the K isotope ratios are close to terrestrial values and ^{39}K is the major isotope (93.2 % isotope abundance), it can be assumed that essentially all ^{39}K is either native or from contamination and only a negligible amount is cosmogenic. With this assumption and based on the measured ^{39}K signals, the expected signals for terrestrial ^{40}K and ^{41}K (native + contamination) can be calculated. This calculation was done for each individual measurement cycle. For this step of the calculation, the $^{41}K/^{39}K$ and $^{40}K/^{39}K$ ratios resulting from the standards measured directly before the sample measurement are used to represent the isotope ratio of the contaminant. The thus calculated terrestrial signals were then subtracted from the measured signals and the corrected, i.e., cosmogenic, $(^{40}K/^{41}K)_{cos}$ ratios are plotted against the cycle number or the ^{40}K signal height. An example of this type of data treatment is discussed in Fig. 6b.

3.2. TIMS measurements

The filaments implanted with K and slightly covered with Fe were loaded directly into the sample wheel of the Thermo Fisher® Trition Plus TIMS spectrometer without any addition of an activator. The instrument is the same as the one used by Naumenko et al. (2013) to precisely determine the terrestrial K isotope composition. Terrestrial potassium has $^{41}K/^{39}K = 0.0721677$ and $^{40}K/^{39}K = 0.00\,0125116(57)$, i.e., ^{39}K is by far the most abundant isotope, followed by ^{41}K, and the low-abundance isotope ^{40}K. In contrast, cosmogenic K has $^{41}K/^{39}K$ and $^{40}K/^{39}K$ ratios in the range 0.969 – 1.038 and 0.85 – 0.88, respectively. The measurements were performed using a double filament set-up applying ~ 430 mA to the evaporation filament with the implanted K (start value) and ~ 860 mA to the ionization filament. Potassium-39, ^{40}K, and ^{41}K were measured on Faraday Cups L2, C, and H2, respectively. At the beginning of the project ^{40}K was measured in Faraday cup C, which worked well for standards with more than 1 ng K on the filament. For smaller K amounts and for most of the samples, however, this set-up gave inutile results. Thus, for subsequent measurements, an ion counter instead of the central Faraday Cup was used. Possible interferences from Ca isotopes were controlled by measuring ^{42}Ca in Faraday Cup H3. Faraday Cups L2, H2, and H3 were all connected to 10^{10} Ω resistors.

Due to the often limited sample amounts, focusing and peak centering was performed before the sample measurements using standards. There was, however, a visual inspection on peak centering and peak shape before the sample measurement. The instrument is stable enough and the set-up is reproducible enough that the samples can be measured in the same configuration as the standard measured directly before the samples. If sample ^{40}K was measured using the ion counter, also ^{40}K from the standard measured before the sample was measured using the ion counter. As not to lose any K, the isotope ratio measurements for the samples started already during the heating-up phase of the filaments after the first signals were detected.

For standard measurements, typically 500 cycles were measured with a single cycle integrating the signal for 4.32 s. Thanks to the stability of the signal, the number of cycles was sufficient for obtaining high precision isotope ratios. The measurements for the samples lasted for as long as there was a measurable signal (usually > 1–2 mV on a Faraday) or after a sufficient number of stable data were collected. In doing so, up to 3000 consecutive cycles were measured. The baseline was measured at the end of the measurement. Typical ^{39}K and ^{41}K signal strengths for the samples are in the range of a few V and a few 100 mV, respectively. For some cycles, however, signal strengths can reach a few tens of V and a few V for ^{39}K and ^{41}K, respectively.

The abundance sensitivity of the Triton Plus TIMS is good enough so that no effects from the tailing of the large ^{39}K signal onto the ^{40}K signal is measurable (e.g., Naumenko et al., 2013; Amelin and Merle, 2021). Therefore, no corrections are required. Other possible parameters compromising the signal are isobaric interferences, which are especially problematic for the low abundance isotope ^{40}K. Interferences, from molecular ions of unknown nature and especially from ^{40}Ca, can result in anomalous peak shapes and irregular fractionation patterns. Interferences from ^{40}Ca can be ruled out, because they are expected to grow with increasing filament temperature due to the lower volatility of Ca compared to K, which results in significantly higher evaporation currents than usually applied during K measurements. Consequently, ^{40}Ca interferences would be more pronounced at the end of the run. However, no such effects were observed in the measurements. In addition, the ^{42}Ca signals were monitored and were always negligible. In contrast, molecular interferences are expected to be more pronounced at the beginning of the measurements at low filament currents. No such effects were observed either. As a conclusion, isobaric interferences can be neglected for the measurements performed in this study.

3.3. TIMS-measurements – Standards

All standard measurements were performed using the standard reference material SRM 3141a, which has a K concentration of 0.16 mol/L in a solution containing HNO_3 at a volume fraction of 1 %. The dissolution steps to prepare 100 ng/µl, 50 ng/µl, 25 ng/µl, 5 ng/µl, 1 ng/µl, and 0.5 ng/µl standards were all performed using solutions with a HNO_3 volume fraction of 1 %. From these (diluted) K standard solutions, 1 µl was loaded onto a rhenium filament and dried down. Standard material was not processed and homogenized with the metal in the crucible and was not extracted using electric fields. Consequently, standard

and sample measurements are not directly comparable. However, since large isotope shifts are expected, minor differences caused by the different treatments of standards and samples can be ignored. As another difference, the standards were not measured using the total evaporation method but with a number of cycles that are sufficient to obtain high precision isotope ratios. Typically, the standards were measured in 500 cycle set-ups.

To check the procedure for reliability, dilution series with standards ranging from 100 ng to 1 ng K on the filament were performed. The results are compiled in Table 1. The measurements for the 100 ng, 50 ng, 25 ng, 5 ng, and 1 ng standards were performed using Faraday detectors for all three K isotopes. The ^{40}K measurements for the 1 ng standards are too close to the baseline, rendering them unreliable. The reproducibility's, given by the 2σ-standard deviation of the weighted mean, for the ^{41}K/^{39}K ratios are 0.028 %, 0.029 %, 0.052 %, 0.013 %, and 0.029 % for the 100 ng, 50 ng, 25 ng, 5 ng, and 1 ng standards, respectively. The reproducibility's for ^{40}K/^{39}K are 0.22 % (100 ng), 0.19 % (50 ng), 0.27 % (25 ng), and 0.04 % (5 ng).

Fig. 4 depicts the readings for ^{40}K (in V, Fig. 4a) and the ^{40}K/^{39}K (Fig. 4b) and ^{41}K/^{39}K (Fig. 4c) ratios for a measurement using 100 ng K on the filament. The standard was measured using the central cup as a Faraday detector. The readings for ^{40}K are relatively stable, the 2σ standard deviation considering all measurements is ∼ 11 % (for ∼ 11 pg ^{40}K on the filament). The individual ^{40}K/^{39}K and ^{41}K/^{39}K ratios together with their averages (solid line), and the 2σ standard deviations (grey area) are shown in panels b and c, respectively. The scatter for ^{40}K/^{39}K is too large to discern a trend. For ^{41}K/^{39}K, however, there might be a slight trend of decreasing ratios with advance of the measurement. This trend is opposite to what is expected for *mdf* effects. A trend dominated by *mdf* effects produces light isotope ratios at the beginning of the measurement that grow heavier throughout the measurement, i.e., opposite to what is seen in Fig. 4. The overall pattern could be described as reverse fractionation due to potential reservoir effects, e.g., a new, thus far unfractionated K reservoir, is activated, contributes to the measurement, and therefore produces slope reversals.

There is a slight trend that the ^{41}K/^{39}K ratios become heavier with decreasing amount of standard material loaded onto the filament. The average ^{41}K/^{39}K ratios for the 100 ng, 50 ng, 25 ng, 5 ng, and 1 ng standard measurements are (in 10^{-2}): 7.19816(205), 7.20296(788), 7.21060 (355), 7.22669(97), and 7.22288(208), respectively. The values in the brackets give the 2σ standard deviation relative to the last relevant digits. The ^{41}K/^{39}K ratios become heavier by ∼ 0.35 % from 100 ng to 1 ng. There are two possible explanations for this finding. First, an instrumental *mdf* that changes slightly with sample amount. For the 100 ng standards, the instrumental *mdf* is −0.13 %/amu. Essentially the same fractionation is calculated for the 50 ng standards (−0.09 %/amu). For the 25 ng standards the fractionation is reduced to −0.04 %/amu. The situation is slightly reversed for the 5 ng standard measurements. The instrumental *mdf* is + 0.07 %/amu and for the 1 ng standard, the instrumental *mdf* is + 0.04 %/amu. No such trend is visible for the ^{40}K/^{39}K ratios, the (average) isotope ratios for the 100 ng, 50 ng, 25 ng, and 5 ng standards are (in 10^{-4}) 1.23883(262), 1.24050(240), 1.24269(498), and 1.23795(407), respectively. The 1 ng measurement cannot be used for this discussion, because ^{40}K was measured on a Faraday detector, resulting in signals indistinguishable from the baseline. The grand average ^{40}K/^{39}K ratio considering all standard measurements from 100 ng to 5 ng (in 10^{-4}) is 1.23985(146) corresponding to mass fractionation factor of −0.9 %/amu.

Since the standards were measured with a similar number of cycles (see above), the larger K amount of the 100 ng standard is at the end of the measurement much less exhausted than the much smaller amount of the 1 ng standard. Consequently, a 100 ng standard running for much longer and reaching a similar level of exhaustion than the 1 ng standard might at the end produce a very similar fractionation pattern.

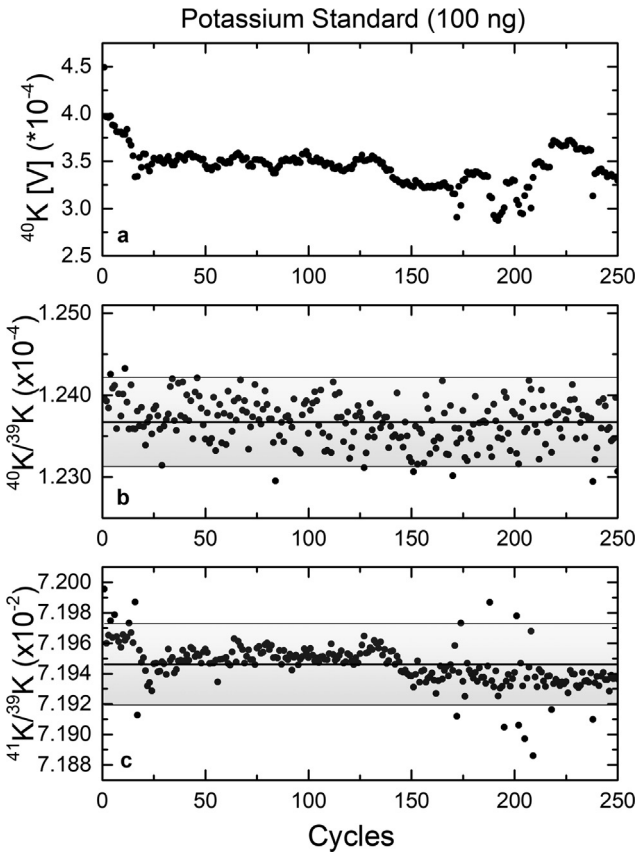

Fig. 4. ^{40}K readings (in V, upper panel), ^{40}K/^{39}K ratios (middle panel), and ^{41}K/^{39}K ratios (lower panel) for a K standard measurement using 100 ng K. The ratios have not been corrected for instrumental mass fractionation. The average values and their 2σ standard deviations are shown by the solid black lines and the grey areas, respectively.

To summarize, the averaged $^{41}K/^{39}K$ ratios become slightly heavier with smaller K amounts on the filament. This finding could indicate that there is a slight dependence of the instrumental *mdf* on the sample amount. Fractionation reversals have also been observed by Amelin and Merle (2021). These authors attribute the effect either to reservoir mixing between variably fractionated domains in the sample load or to emission of natural K from the filament material. The latter can be excluded for this study because measurements of empty filaments gave very low signals (see below). Another possible explanation are minor contributions from unknown interferences. Since there is no measurable effect on the $^{40}K/^{39}K$ ratios, the hypothetical interference would be on ^{41}K. In the present study, however, the effect is small, i.e., in the range of a few %, and therefore not relevant for the study of K isotopes in iron meteorites. For example, the (weighted) average $^{41}K/^{39}K$ ratio considering all standards is 0.0721896 ± 0.0000504. The 2σ standard deviation is 0.06 %. This effect is negligible because the cosmogenic K isotope ratios are vastly different from terrestrial ratios (see also Fig. 3). Important is the finding that K isotope ratios can be measured reproducibly and reliably even with small sample amounts.

3.4. TIMS-measurements – Blanks

Each measurement campaign comprised a blank measurement, i.e., a filament that was processed like a sample extraction but without any sample in the crucible. In addition, after sample extraction, there is the re-extraction, i.e., the filament loaded with the sample K is replaced by a new filament, the already processed sample is heated again, and the voltage between the sample and the filament is again set to 4 kV. For some samples, the re-extractions gave K signals above the blank levels, but most of the re-extractions are consistent with blanks. However, quantifying the blank was not possible because no spikes were used for the TIMS measurements as not to contaminate and compromise the spectrometer and adding and equilibrating spike is almost impossible considering the way the K is extracted from the sample.

The data is not evaluated in the standard way via isotope ratios corrected for blanks and instrumental mass fractionation. Instead, the data is evaluated in a mixing diagram, plotting $^{40}K/^{39}K$ as a function of $^{41}K/^{39}K$. In such a plot, the slope of the (correlated) data gives the $^{40}K/^{41}K$ ratio, which is the ratio used for CRE studies. For this approach to be reliable, it is essential that there are not more than two different K components on the filament. Very likely there is one component with terrestrial (or very close to terrestrial) K isotope composition. This component can be remaining terrestrial contamination and/or native K from the sample. The latter might be K from troilite inclusions. Such K is expected to have terrestrial or close to terrestrial isotope composition because volatile elements are not expected to show large nucleosynthetic anomalies. While the sample preparation procedure is designed to minimize contamination, native K from within the sample cannot be avoided.

The amount of blank in the analyses is low. First, the ^{39}K blank signals for the various sessions performed in this study range from 0 to 3×10^{-9} A, with an average of $(8 \pm 10) \times 10^{-10}$ A. In comparison, the 1 ng standard measurement gave a ^{39}K signal of up to 1×10^{-8} A. Second, much higher currents were needed for the evaporation and the ionization filaments of the blank measurements than for the sample and standard measurements. There is essentially no blank signal from the evaporation filament at a typical heating current of ∼ 430 mA; during blank measurements the signal started at filament currents higher than ∼ 500 mA. Third, the isotope ratios for the blanks are consistent with terrestrial values. These findings give confidence that the entire blank of the extraction system including the TIMS measurements is low and that the isotope ratios are close to terrestrial.

4. First K isotope data

Eight measurements of the four different meteorite samples (including one mixture) were performed using different settings and/or different versions of the extraction system. During the project, the extraction system evolved from version 1 to version 4, always with the goal to extract enough cosmogenic K for reliable TIMS measurements. Table 2 gives a compilation showing which sample has been measured with which specific setting. As we were focusing for most of the project on having enough K on the filament for isotope ratio measurements, sometimes K collection started too early resulting in the collection of too large amounts of native K, i.e., the separation of cosmogenic from native K was not sufficient. Table 3 gives a short summary of the studied iron meteorites, the total recovered masses, CRE ages, and the shielding indicators $^{4}He/^{21}Ne$.

4.1. Meteorite measurements – First results for Casas Grandes

The measurement campaign started with the IIIAB iron meteorite Casas Grandes, found 1867 in Mexico. The recovered mass of 1.55 ton indicates that this meteorite was most likely a large object in space, thus the amount of cosmogenic K is expected to be low in such a large object. The measurement campaign consisted of two standard measurements (100 ng K), the sample filament, the filament collecting the re-extraction, and a blank. In the early phase of the study, ^{39}K, ^{40}K, and ^{41}K were all measured on Faraday detectors, which rendered the ^{40}K measurements difficult and uncertain. The results are summarized in Table 4.

Blanks were low and hardly produced any measurable signal. In addition, the $^{40}K/^{39}K$ and $^{41}K/^{39}K$ ratios of the blanks, though within large uncertainties, are close to terrestrial ratios. The results for the two standard measure-

Table 2
Versions and set-ups used for sample extractions.

Version	Crucible & Inlet (Specials)	Distance Filament −Sample (cm)	Heating current (A)	Samples
Version 1	Tantalum & Graphite	8	195	Casas Grandes, first Casas Grandes, multiple Grant Nantan − 1
Version 2	Molybdenum & Graphite	6	245	Nantan − 2 Meteorite mixture
Version 3	Molybdenum & BN	8	245	Kayakent
Version 4	Molybdenum & BN (Dome)	8	245	Casas Grandes

The two samples Nantan − 1 and Nantan − 2 are not discussed because the data are unreliable likely due to the large pre-atmospheric size of Nantan and its short CRE age (Weber et al., 1986).

Table 3
Total known mass, CRE ages, and $^{4}He/^{21}Ne$ ratios for the studied iron meteorites.

Sample	Total known mass [t]	CRE age [Myrs]	$^{4}He/^{21}Ne$
Casas Grandes	1.55	437 ± 109	569
Grant	0.525	642 ± 56	297 – 347
Nantan	9.5	68 ± 50	596
Kayakent	0.085	52 ± 3	233
Davis Mountains	0.689	415 ± 29	277
Kenton County	0.194	652 ± 99	394
Sandtown	0.00935	465 ± 33	229

The CRE ages and $^{4}He/^{21}Ne$ ratios are from Smith et al. (2019), except for the $^{4}He/^{21}Ne$ ratio for Grant, which is from Lavielle et al. (1999) and the CRE age and the $^{4}He/^{21}Ne$ ratio for Nantan, which is from Weber et al. (1986).

ments agree; though only because the uncertainty of the $^{40}K/^{39}K$ ratio for the second standard (Std-2) is large (Table 4). The uncertainty-weighted averages for the two standard measurements are $^{40}K/^{39}K = (1.282 \pm 0.097) \times 10^{-4}$ and $^{41}K/^{39}K = (7.261 \pm 0.022) \times 10^{-2}$. The instrumental mass fractionation for $^{41}K/^{39}K$ is ~ 2.5 %/amu and ~ 0.3 %/amu for $^{40}K/^{39}K$.

Fig. 5 depicts the meteorite data in a $^{40}K/^{39}K$ vs. $^{41}K/^{39}K$ diagram. There is a clear trend in the data, starting with $^{40}K/^{39}K$ and $^{41}K/^{39}K$ ratios similar to or only slightly higher than the terrestrial standards before they increase almost linearly and reach final values significantly higher than the standards. This trend is clearly distinct from the *mdf*-line. The normal average $^{40}K/^{39}K$ and $^{41}K/^{39}K$ ratios are $(1.314 \pm 1.052) \times 10^{-3}$ and $(7.455 \pm 0.224) \times 10^{-2}$, respectively. Using the integrated signals, the $^{40}K/^{39}K$ and $^{41}K/^{39}K$ ratios are 1.221×10^{-3} and 7.446×10^{-2}, respectively, i.e., within the uncertainties identical to the normal averages. The individual data for Casas Grandes define a linear array connecting the terrestrial ratio with cosmogenic K. By determining a linear correlation and forcing the line through the weighted average for the two standard measurements, the calculated slope corresponding to the $^{40}K/^{41}K$ ratio is 0.571 ± 0.003 (R = 0.967, shown by the dotted line in Fig. 5). The slope of this correlation line is shallower than the slope of the calculated mixing line (slope ~ 0.9, solid line). This discrepancy might indicate that in addition to mixing, the data are also fractionated (fractionation favoring light isotopes results in a shallower slope). Another explanation could be that the cosmogenic endmember composition is not as assumed, when calculating the mixing line (at least not for Casas Grandes). Accordingly, the $^{40}K/^{41}K$ ratio of 0.571 ± 0.003 (not corrected for fractionation) determined in the present study is significantly lower than the expected range of 0.85 – 0.88 suggested by Voshage (1967).

The apparently low cosmogenic $^{40}K/^{41}K$ ratio of 0.571 ± 0.003 is confirmed by another way of data treatment. Since all measured ratios are close to terrestrial, a simple two-component mixing calculation assuming all ^{39}K to be terrestrial, can also be used to calculate cosmogenic $^{40}K/^{41}K$ ratios. Performing this mixing calculation for each individual measurement cycle gives time dependent $^{40}K/^{41}K$ ratios with values as high as ~ 2 at the beginning of the measurement. After ~ 600 cycles, a long and stable plateau with constant $(^{40}K/^{41}K)_{cos} = 0.573 \pm 0.010$ forms up to cycle number 1100 (shown by the filled gray circles in Fig. 5). At the end of the measurement, the $(^{40}K/^{41}K)_{cos}$ ratios drop to lower values. The resulting ratio is in excellent agreement with the value obtained from fitting the data in the $^{40}K/^{39}K$ vs. $^{41}K/^{39}K$ diagram (Fig. 5).

After sample extraction, a second extraction at a slightly higher temperature was performed to check if all sample K had been extracted in the first heating step (Casas Grandes Re, Table 4). The integrated signal of the re-extraction was much larger than the integrated blank signal; however, it

Table 4
K isotope ratios for Casas Grandes and Grant.

Sample	$^{41}K/^{39}K$	$^{40}K/^{39}K$	$^{40}K/^{41}K$
Casas Grandes – First			
Std-1	$(7.303 \pm 0.049) \times 10^{-2}$	$(1.280 \pm 0.097) \times 10^{-4}$	
Std-2	$(7.245 \pm 0.031) \times 10^{-2}$	$(1.819 \pm 1.814) \times 10^{-4}$	
Average Standard	**$(7.261 \pm 0.022) \times 10^{-2}$**	**$(1.282 \pm 0.097) \times 10^{-4}$**	
Casas Grandes, normal average	$(7.455 \pm 0.224) \times 10^{-2}$	$(1.314 \pm 1.052) \times 10^{-3}$	
Casa Grandes, integrated signal	7.446×10^{-2}	1.221×10^{-3}	
Slope via linear fit			0.571 ± 0.003
Assuming all ^{39}K is terrestrial			0.573 ± 0.010
Casas Grandes − Re	$(7.370 \pm 0.335) \times 10^{-2}$	$(5.3 \pm 20.6) \times 10^{-4}$	
Casas Grandes, Summary	**7.446×10^{-2}**	**1.221×10^{-3}**	**0.571 ± 0.003**
Casas Grandes – Multiple			
Std-1 (100 ng)	$(7.162 \pm 0.086) \times 10^{-2}$	$(1.246 \pm 0.004) \times 10^{-4}$	
Std-2 (100 ng)	$(7.178 \pm 0.058) \times 10^{-2}$	$(1.251 \pm 0.005) \times 10^{-4}$	
Average Standard	**$(7.173 \pm 0.048) \times 10^{-2}$**	**$(1.248 \pm 0.003) \times 10^{-4}$**	
Casas Grandes, normal average	$(7.268 \pm 0.060) \times 10^{-2}$	$(4.015 \pm 0.398) \times 10^{-4}$	
Casas Grandes, integrated signal	7.258×10^{-2}	4.085×10^{-4}	0.332
Assuming all ^{39}K is terrestrial			0.36 ± 0.14
Casas Grandes 1.Re, normal average	$(7.129 \pm 0.130) \times 10^{-2}$	$(7.988 \pm 0.117) \times 10^{-4}$	n.d.
Casas Grandes 1.Re, integrated signal	7.248×10^{-2}	5.056×10^{-4}	0.504
Casas Grandes 2.Re, normal average	$(7.259 \pm 0.122) \times 10^{-2}$	$(1.606 \pm 0.624) \times 10^{-4}$	0.041
Casas Grandes 2.Re, integrated signal	7.266×10^{-2}	1.594×10^{-4}	0.037
Casas Grandes, Summary	**7.248×10^{-2}**	**5.056×10^{-4}**	**0.504**
Grant			
Std-1 (100 ng)	$(7.174 \pm 0.009) \times 10^{-2}$	$(1.249 \pm 0.005) \times 10^{-4}$	
Std-2 (100 ng)	$(7.158 \pm 0.021) \times 10^{-2}$	$(1.246 \pm 0.004) \times 10^{-4}$	
Std-3 (100 ng)	$(7.151 \pm 0.018) \times 10^{-2}$	$(1.244 \pm 0.006) \times 10^{-4}$	
Average Standard	**$(7.168 \pm 0.008) \times 10^{-2}$**	**$(1.247 \pm 0.003) \times 10^{-4}$**	
Grant-1, normal average	$(7.229 \pm 0.018) \times 10^{-2}$	$(1.876 \pm 0.067) \times 10^{-4}$	0.103 ± 0.046
Grant-1, integrated signal	7.246×10^{-2}	1.893×10^{-4}	0.083
Assuming all ^{39}K is terrestrial			0.098 ± 0.048
Grant-1 (first readings)	$(7.256 \pm 0.004) \times 10^{-2}$	$(2.056 \pm 0.034) \times 10^{-4}$	0.092 ± 0.014
Grant-1, Summary	**$(7.255 \pm 0.039) \times 10^{-2}$**	**$(2.016 \pm 0.042) \times 10^{-4}$**	**0.093 ± 0.013**
Grant-2, normal average	$(7.293 \pm 0.118) \times 10^{-2}$	$(1.820 \pm 0.040) \times 10^{-4}$	0.046 ± 0.046
Grant-2, integrated signal	7.288×10^{-2}	1.828×10^{-4}	0.048
Assuming all ^{39}K is terrestrial			0.030 ± 0.006
Grant-2 (first readings)	$(7.273 \pm 0.074) \times 10^{-2}$	$(1.948 \pm 0.188) \times 10^{-4}$	0.067 ± 0.055
Grant-2, Summary	**$(7.279 \pm 0.062) \times 10^{-2}$**	**$(1.826 \pm 0.038) \times 10^{-4}$**	**0.031 ± 0.006**
Dilution Series			
Std-1 (0.5 ng)	$(7.208 \pm 0.475) \times 10^{-2}$	$(1.523 \pm 0.221) \times 10^{-4}$	
Std-2 (1.0 ng)	$(7.290 \pm 0.544) \times 10^{-2}$	$(1.439 \pm 0.250) \times 10^{-4}$	
Std-3 (1.0 ng)	$(7.192 \pm 0.098) \times 10^{-2}$	$(1.506 \pm 0.097) \times 10^{-4}$	
Std-4 (1.0 ng)	$(7.201 \pm 0.207) \times 10^{-2}$	$(1.542 \pm 0.134) \times 10^{-4}$	
Std-5 (1.0 ng)	$(7.204 \pm 0.030) \times 10^{-2}$	$(1.546 \pm 0.036) \times 10^{-4}$	
Std-6 (Stock) (^{40}K on Faraday)	$(7.202 \pm 0.002) \times 10^{-2}$	$(1.248 \pm 0.007) \times 10^{-4}$	
Std-7 (Stock)	$(7.200 \pm 0.002) \times 10^{-2}$	$(1.389 \pm 0.070) \times 10^{-4}$	
Std-8 (Stock)	$(7.203 \pm 0.001) \times 10^{-2}$	$(1.486 \pm 0.037) \times 10^{-4}$	
Average Standard	**$(7.203 \pm 0.001) \times 10^{-2}$**	**$(1.248 \pm 0.007) \times 10^{-4}$**	

was only ~ 5 % of the total integrated sample signal. The isotope ratios indicate that K from the re-extraction was a mixture of terrestrial and cosmogenic K.

To summarize, the $^{40}K/^{39}K$ and $^{41}K/^{39}K$ ratios for Casas Grandes are close to terrestrial K, cosmogenic K is detectable, but is difficult to quantify. For ^{40}K, the cosmogenic contribution is in the range 70–80 %, but for ^{41}K more than 95 % of the signal is terrestrial. It was therefore decided to analyze another Casas Grandes sample after changing the extraction procedure to evaluate whether all cosmogenic K had been extracted.

4.2. Meteorite measurements – Multiple K extractions for Casas Grandes

The measurement campaign consists of two standards (100 ng), a blank, the analysis of a Casas Grandes sample, and two re-extractions to check for complete K extraction. During the two re-extraction steps the temperature was periodically cycled up and down by 10 A (~50 °C) to stir the material from the lower part of the crucible to the upper part to enhance K extraction. The results are given in Table 4. The two standards agree to within ~ 0.3 %

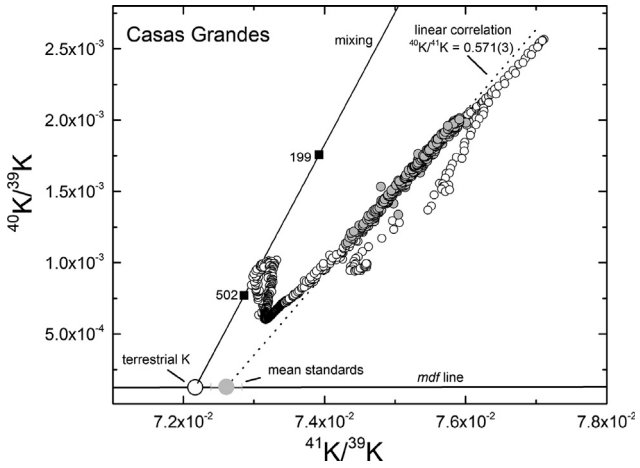

Fig. 5. $^{40}K/^{39}K$ as a function of $^{41}K/^{39}K$ for the (first) Casas Grandes measurement campaign. The solid line is the calculated mixing line between terrestrial and cosmogenic K. The dashed line is the correlation (forced through the average ratio for the standards (gray filled circle) calculated from the individual ratios (open symbols). The slope of this correlation line corresponds to the $^{40}K/^{41}K = 0.571 \pm 0.003$ (R = 0.967). Also shown is the mass-dependent fractionation line (*mdf*). The cycles from 600 to 1100 are shown by filled gray circles.

and ~ 0.4 % for $^{41}K/^{39}K$ and $^{40}K/^{39}K$, respectively, and the fractionation is −0.25 %/amu for $^{40}K/^{39}K$ and −0.30 %/amu for $^{41}K/^{39}K$.

The results for the first extraction from Casas Grandes are $^{40}K/^{39}K = (4.015 \pm 0.398) \times 10^{-4}$ and $^{41}K/^{39}K = (7.268 \pm 0.060) \times 10^{-2}$ (normal averages) or $^{40}K/^{39}K = 4.085 \times 10^{-4}$ and $^{41}K/^{39}K = 7.258 \times 10^{-2}$ (integrated signal), i.e., they are both higher than the standard by ~ 3σ and by more than a factor of ~ 3. Since the ratios also deviate from the *mdf*-line, the data shows a clear cosmogenic signal. The $(^{40}K/^{41}K)_{cos}$ ratio is 0.332, calculated using the correlation between the ratios for the standards and the integrated signals. Assuming all ^{39}K to be terrestrial and correcting ^{40}K and ^{41}K accordingly results in $(^{40}K/^{41}K)_{cos}$ ratios varying between ~ 0.5 at the very beginning and very end of the measurement and ~ 0.2 at the middle of the measurement. The grand average using all ratios is 0.36 ± 0.14. For the last ~ 80 cycles at the very end of the measurement, there is a small plateau of almost constant $(^{40}K/^{41}K)_{cos}$ ratios, with an average of 0.62 ± 0.01.

After sample extraction, a second extraction was performed (Casas Grandes – 1.Re in Table 4). The $^{41}K/^{39}K$ and $^{40}K/^{39}K$ ratios of 7.248×10^{-2} and 5.056×10^{-4} (integrated signals) are ~ 3σ and a factor of 4, respectively, higher than the terrestrial ratios. The $(^{40}K/^{41}K)_{cos}$ ratio of this second extraction is 0.505, i.e., even slightly higher than the ratio of the sample extraction, but consistent with the first sample. The integrated ^{39}K signal of the first re-extraction was ~ 30 % of the integrated signal of the first sample extraction, i.e., there was still some cosmogenic and native K in the sample after the first extraction. Considering the $(^{40}K/^{41}K)_{cos}$ ratios, the cosmogenic contribution was even slightly higher, while the total amount of K in the second extraction was lower than in the first sample extraction.

A second re-extraction (Casas Grandes 2nd-Re) was performed, which gave $^{41}K/^{39}K$ and $^{40}K/^{39}K$ ratios indistinguishable from the standard within 2σ uncertainties. The data therefore indicate that the extraction was not complete after the first heating step, but that after the second heating step, i.e., after the first re-extraction, most of the K had been extracted. The finding that the amount of cosmogenic K relative to native K is higher in the re-extraction step than in the first sample extraction agrees with the study of Voshage and Hintenberger (1959), who argued that heating the sample for ~ 30 min at a temperature slightly below the melting point significantly reduces K contamination without affecting the amount of cosmogenic K.

Assuming that the highest $(^{40}K/^{41}K)_{cos}$ ratio best reflects the true cosmogenic ratio, the $^{40}K/^{41}K$ ratio of 0.505 obtained in the first re-extraction step agrees well with the data obtained for the first Casas Grandes sample (0.571 ± 0.003, 0.573 ± 0.010).

To summarize, the results for the second Casas Grandes measurements are in good agreement with the data for the first Casas Grandes samples, confirming the reproducibility of the extraction and data handling procedure. The data also indicate that in the first extraction step the ratio of native/cosmogenic K was higher than the second extraction step.

4.3. Meteorite measurements – Grant

Two aliquots of the IIIAB iron meteorite Grant were studied. Following the results from the second extraction experiment on Casas Grandes, the extraction was performed using periodic heating of the sample. The results are given in Table 4 and are shown in Fig. 6. In addition to the sample measurements, also three K standards (100 ng) were measured to determine instrumental mass fractionation. The data for all three standards agree within uncertainties. The weighted average $^{41}K/^{39}K$ and $^{40}K/^{39}K$ ratios are $(7.168 \pm 0.008) \times 10^{-2}$ and $(1.247 \pm 0.003) \times 10^{-4}$, respectively, which corresponds to a mass-dependent fractionation of about −0.35 %/amu.

Fig. 6a depicts $^{40}K/^{39}K$ as a function of $^{41}K/^{39}K$, the average ratios for the standards, the individual data for the two Grant samples, the ratios for the integrated signals, and the *mdf*-line. All $^{40}K/^{39}K$ and most of the $^{41}K/^{39}K$ ratios for Grant-1 and Grant-2 deviate from the terrestrial values, showing a clear cosmogenic signal. In contrast to Casas Grandes, however, there is no linear trend of the individual $^{40}K/^{39}K$ and $^{41}K/^{39}K$ ratios for either of the two Grant samples. Calculating the ratios using integrated signals results in $^{40}K/^{39}K = 1.893 \times 10^{-4}$ for Grant-1 and $^{40}K/^{39}K =$ and 1.828×10^{-4} for Grant-2. For $^{41}K/^{39}K$ the integrated ratios are 7.246×10^{-2} for Grant-1 and 7.288×10^{-2} Grant-2, (shown by the gray squares in

Fig. 6a). Calculating the $^{40}K/^{41}K$ ratios from the integrated signals gives low values of 0.083 for Grant-1 and 0.048 for Grant-2.

Assuming all measured ^{39}K to be either native or from terrestrial contamination and calculating individual $(^{40}K/^{41}K)_{cos}$ ratios for each measurement cycle gives the results shown in Fig. 6b. The $(^{40}K/^{41}K)_{cos}$ ratios for Grant-2 start at a value of ~ 0.05, increasing up to ~ 0.25 before slowly declining and reaching a very short plateau at the end of the measurement. The $(^{40}K/^{41}K)_{cos}$ value of the plateau, which is from cycles 200 to 230 is 0.030 ± 0.006. For sample Grant-1 there is no clear trend, the $(^{40}K/^{41}K)_{cos}$ ratios vary widely between ~ 0.04 and ~ 0.15, the average value is 0.0978 ± 0.049. The $(^{40}K/^{41}K)_{cos}$ ratios calculated this way for Grant-1 and Grant-2 are almost indistinguishable from the values obtained using integrated signals. However, the $(^{40}K/^{41}K)_{cos}$ ratios determined in this way are significantly lower than the ratio of 0.85 – 0.88 proposed by Voshage (1967).

For some of the Grant-1 and especially for most of the Grant-2 data shown in Fig. 6a, there is a linear trend almost parallel to the *mdf*-line, indicating mass dependent fractionation. If we assume that the start of the measurement produces the least fractionated signal, which might not strictly be true as the early phase of a measurement often produces slightly lighter isotope ratios, $^{41}K/^{39}K$ and $^{40}K/^{39}K$ ratios can also be calculated using only the first, e.g., 10–100 readings. For the Grant data, this assumption is supported by the observation that the first readings show no trend, scatter around a given value, and are therefore indeed less affected by fractionation. The results for Grant-1 and Grant-2 are: $^{40}K/^{39}K = (2.056 \pm 0.034) \times 10^{-4}$ and $^{41}K/^{39}K = (7.256 \pm 0.004) \times 10^{-2}$ and $^{40}K/^{39}K = (1.948 \pm 0.188) \times 10^{-4}$ and $^{41}K/^{39}K = (7.273 \pm 0.074) \times 10^{-2}$, respectively. The resulting $^{40}K/^{41}K$ ratios for Grant-1 are 0.092 ± 0.014 and 0.067 ± 0.055 for Grant-2. The values agree within the uncertainties with the ratios obtained before.

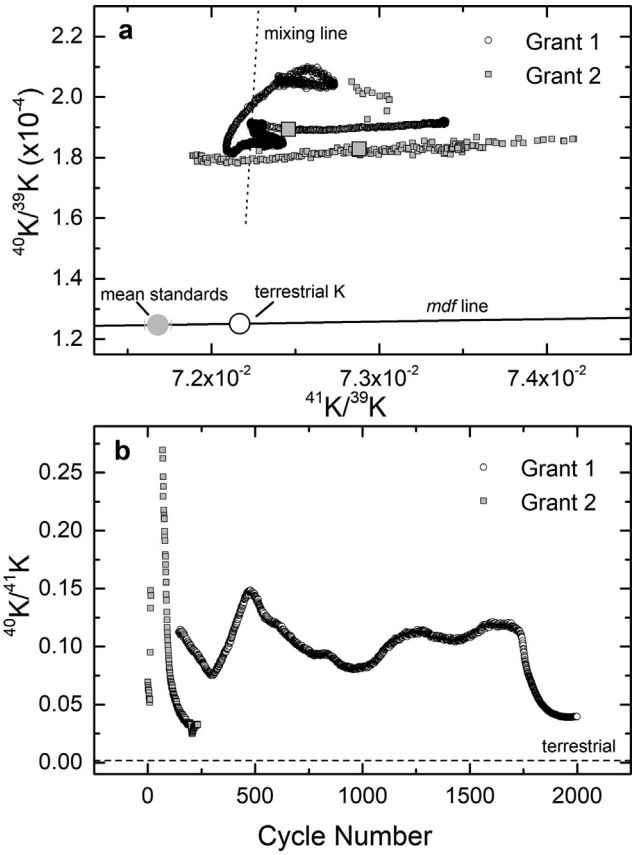

Fig. 6. $^{40}K/^{39}K$ as a function of $^{41}K/^{39}K$ for the two Grant samples. For explanation see Fig. 5. The gray squares are the ratios calculated from integrated signals (panel a). $^{40}K/^{41}K$ as a function of measurement cycle for the two Grant samples (panel b). The $^{40}K/^{41}K$ has been calculated by assuming all measured ^{39}K is from terrestrial contamination. For sample Grant-2 after ~ 400 cycles a relatively constant $^{40}K/^{41}K$ ratio of 0.04157 ± 0.00325 (1σ standard deviation) is reached. The dashed line gives the terrestrial ratio (as measured for the standards). Grant-1 has been measured for more than 100 cycles, but the last readings were all below 1 mV and were therefore rejected.

4.4. Meteorite measurements – A mixture of Davis Mountain, Kenton County, and Sandtown

For each extraction procedure, 5–6 g of sample material is needed, which, after leaching, leaves about 3–4 g for melting and K extraction. This large amount of sample material limits the choices of meteorites to study. The results so far were not fully satisfying because essentially all measured ratios were (too) close to terrestrial. Since it was not clear whether this was due to the choice of the studied meteorite (large objects) or a limitation of the extraction procedure, it was decided to mix three meteorites into one sample with the goal to extract enough cosmogenic K. The goal of this extraction was to study and improve technical aspects of the procedure. The K isotope ratio for a meteorite mixture cannot be used to determine meaningful CRE ages. The three meteorites are Davis Mountains (IIIAB), Kenton County (IIIAB), and Sandtown (IIIAB). All three meteorites have been studied before for their terrestrial ages and their CRE ages (Smith et al., 2019). The CRE ages are 415 ± 29 Ma, 652 ± 99 Ma, and 465 ± 33 Ma for Davis Mountains, Kenton County, and Sandtown, respectively, indicating high amounts of cosmogenic nuclides. The results are compiled in Table 5. The campaign was accompanied by a dilution series using standards with 0.5 ng to 100 ng of K on the filament. For this dilution series we also used the ion counter for ^{40}K measurements. In contrast to the earlier stages of the study, there is no dependence of the $^{41}K/^{39}K$ or $^{40}K/^{39}K$ ratios on the amount of K on the filament (Table 5). The weighted averages are $^{41}K/^{39}K = (7.202 \pm 0.001) \times 10^{-2}$ and $^{40}K/^{39}K = (1.503 \pm 0.023) \times 10^{-4}$ (using only ion counter measurements for ^{40}K). In contrast to the dilution series performed earlier (see above), the standards in this campaign were all measured till exhaustion. Therefore, the effect that exhaustion has on fractionation is similar for all standards and disappears when integral signals are considered.

Table 5
K isotope ratios for the meteorite mixture, Kayakent, and Casa Grandes.

Sample	$^{41}K/^{39}K$	$^{40}K/^{39}K$	$^{40}K/^{41}K$
Mixture			
Std-1 (100 ng)	$(7.169 \pm 0.001) \times 10^{-2}$	$(1.265 \pm 0.010) \times 10^{-4}$	
Std-2 (100 ng)	$(7.163 \pm 0.012) \times 10^{-2}$	$(1.284 \pm 0.010) \times 10^{-4}$	
Std-3 (100 ng)	$(7.145 \pm 0.002) \times 10^{-2}$	$(1.245 \pm 0.013) \times 10^{-4}$	
Average Standard	**$(7.164 \pm 0.001) \times 10^{-2}$**	**$(1.269 \pm 0.009) \times 10^{-4}$**	
Mixture-1, normal average	$(7.188 \pm 0.220) \times 10^{-2}$	$(2.467 \pm 0.214) \times 10^{-4}$	
Mixture, integrated signal	7.206×10^{-2}	2.935×10^{-4}	0.286
Mixture, Summary	**7.206×10^{-2}**	**2.935×10^{-4}**	**0.286**
Kayakent			
Std-1 (0.5 ng)	$(7.439 \pm 0.164) \times 10^{-2}$	$(1.248 \pm 0.064) \times 10^{-4}$	
Std-2 (1 ng)	$(7.174 \pm 0.160) \times 10^{-2}$	$(1.126 \pm 0.082) \times 10^{-4}$	
Std-3 (100 ng) (^{40}K Faraday)	$(7.159 \pm 0.001) \times 10^{-2}$	$(1.245 \pm 0.006) \times 10^{-4}$	
Std-4 (100 ng)	$(7.162 \pm 0.002) \times 10^{-2}$	$(1.256 \pm 0.008) \times 10^{-4}$	
Average Standard	**$(7.160 \pm 0.001) \times 10^{-2}$**	**$(1.249 \pm 0.005) \times 10^{-4}$**	
Kayakent, normal average	$(7.253 \pm 0.047) \times 10^{-2}$	$(4.149 \pm 0.301) \times 10^{-4}$	0.312
Kayakent, integrated signal	7.254×10^{-2}	4.146×10^{-4}	0.440
Assuming all ^{39}K is terrestrial			0.28 ± 0.06
Kayakent, Summary	**7.254×10^{-2}**	**4.146×10^{-4}**	**0.344**
Casas Grandes			
Std (100 ng)	$(7.168 \pm 0.002) \times 10^{-2}$	$(1.247 \pm 0.005) \times 10^{-4}$	
Std (100 ng)	$(7.164 \pm 0.001) \times 10^{-2}$	$(1.265 \pm 0.007) \times 10^{-4}$	
Average Standard	**$(7.165 \pm 0.001) \times 10^{-2}$**	**$(1.254 \pm 0.006) \times 10^{-4}$**	
Casas Grandes-1, normal average	$(7.277 \pm 0.091) \times 10^{-2}$	$(6.961 \pm 0.149) \times 10^{-4}$	
Casas Grandes-1, integrated signal	7.398×10^{-2}	3.929×10^{-4}	0.115
Casas Grandes-2, normal average	$(7.261 \pm 0.115) \times 10^{-2}$	$(1.889 \pm 2.291) \times 10^{-4}$	
Casas Grandes-2, integrated signal	7.372×10^{-2}	3.491×10^{-4}	0.108
Casa Grandes, Summary	**7.385×10^{-2}**	**3.710×10^{-4}**	**0.112**

The measurements of the standards give a mass-dependent fractionation of −0.4 %/amu for $^{40}K/^{39}K$ and −0.5 %/amu for $^{41}K/^{39}K$. The sample measurements were not very stable and drifted significantly, which compromises data interpretation. For the first ~ 1500 measurement cycles, the $^{40}K/^{39}K$ and $^{41}K/^{39}K$ ratios move parallel to the *mdf*-line, indicating mass-dependent fractionation during the measurement. At the very end of the measurement, i.e., after about 1800 cycles, the $^{41}K/^{39}K$ ratio becomes lighter and the $^{40}K/^{39}K$ ratio becomes heavier, the latter even reaching values as high as one shortly before the sample was exhausted. Such behavior cannot be due to a reservoir effect. However, interferences can be ruled out as there was no detectable signal on mass 42, i.e., from ^{42}Ca. Due to the large fractionation effects, integrated signals are more reliable than normal averages. The integrated ratios are $^{41}K/^{39}K = 7.206 \times 10^{-2}$ and $^{40}K/^{39}K = 2.935 \times 10^{-4}$ (Table 5). Again, the values, especially the $^{40}K/^{39}K$ ratio, are significantly higher than the ratios for the standard. The $^{40}K/^{41}K$ ratio calculated by using the linear correlation between sample and the standard gives $^{40}K/^{41}K = 0.286$.

4.5. Meteorite measurements – Kayakent

The earlier measurements were compromised by the ill-behaving graphite liner, which was not only difficult to clean but very often broke either during extraction and/or cleaning. To solve the problem, the inner graphite crucible was replaced by a BN liner (version 3, see Appendix 4). Note that Voshage in his original work (e.g., Voshage and Hintenberger, 1959) used a graphite liner because he expected that graphite is almost free of terrestrial K and that the graphite reduces the melting temperature of iron. After changing the inner crucible, Kayakent (IIIAB) was processed. In addition to the meteorite measurements, this batch also comprised an instrumental blank to check whether the BN crucible is as clean as the graphite liner.

By comparing the instrumental blank, which was obtained by performing the entire extraction procedure, but without processing a sample, with the measurements of an empty filament, the blank of the BN liner is slightly higher than that of the graphite liner. For example, while the ^{39}K blank signal for the graphite liner was $\sim 3 \times 10^{-13}$ A, the blank signal for the BN liner was $\sim 4 \times 10^{-12}$ A. However, the slightly higher blank is easily compensated for by the much better handling. In addition, it can be expected that the blank will decrease over time because the BN liner can be used multiple times. No cross contamination is expected from the small Fe amount remaining in the BN liner after cleaning because this Fe was already molten or even in a gas phase and all K has already been released.

In addition to sample and blank extractions, four standards were measured, one with 0.5 ng, one with 1 ng, and

two with 100 ng K on the filament. The results for the 100 ng standards are very reproducible; the deviations for $^{41}K/^{39}K$ and $^{40}K/^{39}K$ ratios are smaller than ~ 0.05 % and ~ 0.9 %, respectively. The deviations for the 1 ng and the 0.5 ng standards are slightly larger, but considering the uncertainties, the agreement is fair. Combining all four standard measurements to a weighted mean gives 2σ standard deviations of 0.4 % for $^{40}K/^{39}K$ and 0.01 % for $^{41}K/^{39}K$. The (average) ratios correspond to mass dependent fractionation factors of −0.2 %/amu and −0.4 %/amu for $^{40}K/^{39}K$ and $^{41}K/^{39}K$, respectively. All data are summarized in Table 5 and are shown in Fig. 7. The individual sample ratios for the ~ 5000 measurement cycles, shown by the open dots, scatter around the average (solid gray circle), which is $^{40}K/^{39}K = 4.146 \times 10^{-4}$ and $^{41}K/^{39}K = 7.254 \times 10^{-2}$. Both ratios are significantly higher than the standard by ~ 200σ and more than a factor of 3. For the first ~ 3500 measurement cycles, there is no trend in the data. At the end of the measurement, after ~ 3500 cycles, the ratios move parallel to the *mdf*-line towards heavier ratios. Assuming that the least-fractionated data at the beginning of the measurement represent the real isotopic ratios best (see also comments above), changes only slightly the results; the new ratios are $^{40}K/^{39}K = 4.081 \times 10^{-4}$ and $^{41}K/^{39}K = 7.243 \times 10^{-2}$. Calculating the (fully integrated) $(^{40}K/^{41}K)_{cos}$ ratio gives a value of 0.440. Again, no uncertainties can be calculated for ratios obtained from integrated signals. The individual ratios all plot close to the mixing line and the integrated ratios plot almost on the mixing line, indicating the reliability of the data.

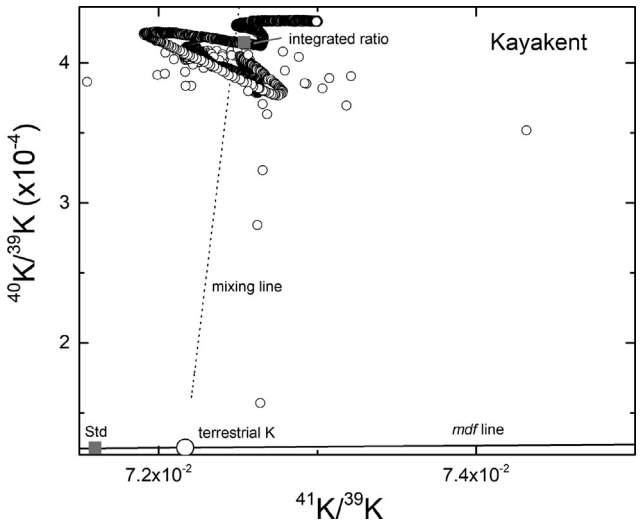

Fig. 7. $^{40}K/^{39}K$ as a function of $^{41}K/^{39}K$ for the Kayakent sample. The average ratio for the standards are shown by the solid grey square. The uncertainties are smaller than the symbol size. The individual readings for the mixed meteorite samples are shown by the open circles and the average ratios (calculated from the integrated signals) are shown by the solid gray circle. Also shown is the *mdf* fractionation line, the ratio for (unfractionated) terrestrial K, and the mixing line between terrestrial and cosmogenic K.

To summarize, a clear cosmogenic signal was detected for Kayakent despite its very low CRE age of only 53 ± 3 Ma (Smith et al., 2019). This gives some confidence in the principal capabilities of the extraction system.

4.6. Meteorite measurements – Casas Grandes (Final)

As the currently latest improvement a (half) spherical cover was added over the filament crucible assembly, which should help the electrical field lines to reach further into the crucible and therefore helps to extract more K from the sample (version 4). Two Casas Grandes samples (IIIAB) were measured in this latest experimental set-up. The results are compiled in Table 5. In addition to the two meteorite samples, the campaign also comprised two standard measurements, each using 100 ng K. The reproducibility is fair, the $^{41}K/^{39}K$ and $^{40}K/^{39}K$ ratios agree within 0.005 % and 1.4 %, respectively. The weighted average ratios for $^{41}K/^{39}K$ are (7.165 ± 0.001) × 10^{-2} (2σ ~ 0.01 %) and (1.254 ± 0.001) × 10^{-2} (2σ ~ 0.37 %) for $^{40}K/^{39}K$. The mass dependent fractionation is slightly inconsistent, it is 0.24 %/amu for $^{40}K/^{39}K$, and −0.36 %/amu for $^{41}K/^{39}K$. The reproducibility for the two Casas Grandes samples is good; the two $^{41}K/^{39}K$ ratios agree within ~ 0.5 % and the $^{40}K/^{39}K$ ratios agree within ~ 12 %. The $^{40}K/^{41}K$ ratios for the two samples are 0.108 and 0.115, demonstrating good reproducibility. All ratios were calculated using integrated signals.

While the data for the two Casas Grandes are reproducible, they differ from the results obtained for the first Casas Grandes samples measured at the beginning of the project. For example, the $(^{40}K/^{41}K)_{cos}$ ratio measured early in the project are ~ 0.5, i.e., significantly higher than the new ratio of ~ 0.10. It might be possible that at least part of this discrepancy is due to sample-sample heterogeneity between the different Casas Grandes chips from our collection.

5. Conclusions and outlook

The first results of this exploratory study to obtain precise and accurate ^{40}K-K CRE ages for iron meteorites are very promising. However, there are still some points that must be addressed and improved before reliable and highly precise ^{40}K-K CRE ages can be determined.

First, the standard measurements with K amounts between 0.5 ng and 100 ng on the filament are reliable and reproducible. The total weighted averages are $^{40}K/^{39}K = (1.245 \pm 0.002) \times 10^{-4}$ (N = 33) and $^{41}K/^{39}K = (7.181 \pm 0.003) \times 10^{-2}$ (N = 44). This corresponds to a reproducible mass-dependent fractionation of −0.43 %/amu for $^{40}K/^{39}K$ and −0.25 %/amu for $^{41}K/^{39}K$.

Second, the blanks are low. Blank extractions resulted in filaments with almost no detectable K. In addition, the very low K signals were obtained only at much higher

evaporation filament currents than used for sample and standard measurements.

Third, it was possible to obtain cosmogenic K isotope signals for almost all iron meteorite samples. However, the measured K isotope ratios are always very close to terrestrial values. Even in the most cosmogenic sample, essentially all ^{39}K is terrestrial and only $\sim$ 5 % of the ^{41}K signal and more than 70 % of the ^{40}K signal was cosmogenic. Considering that there was always sufficient K on the filament, i.e., there was enough K for $\sim$ 1000 (and sometimes even up to $\sim$ 5000) individual readings, it can be concluded that K extraction from the sample and implantation into the filament is efficient. A clear cosmogenic K signal could even be detected for the iron meteorite Kayakent, which has a low CRE age of only 53 $\pm$ 3 Ma (Smith et al., 2019).

Fourth, the limiting factor is rather the large amount of remaining native K than inefficient extraction of cosmogenic K. While the concentrations of native K in iron meteorites are in the range of 40 – 1000 ppb, cosmogenic K concentrations are as low as 1 ppb. Consequently, a typical K isotope measurement in iron meteorites must give ratios close to terrestrial (assuming that native K in iron meteorites has a ratio close to terrestrial) with slight deviations towards cosmogenic values, depending on the exposure ages and the concentration of native K (e.g., Buchwald, 1977; Imamura et al., 1980; Shankar, 2011).

Fifth, increasing the amount of cosmogenic K relative to native K is not possible using wet chemical extraction techniques, but should be possible using the physical extraction system presented here. For example, Voshage and Hintenberger (1959, 1961) argued that pre-heating the sample at a temperature slightly below the melting point significantly reduces K contamination and releases native K from grain boundaries without affecting cosmogenic K. While a pre-heating step was performed, it was not close enough to the melting point and/or not long enough. This pre-heating can easily be improved as it is now clear the K extraction is efficient.

Sixth, the currently limiting factor for the K-isotope measurements in iron meteorites is therefore not the extraction system, it is the unstable signal during the TIMS measurements. To improve on this, a more rigorous total evaporation approach (TE-TIMS) will be used in the follow-up study. In addition, there is a need to better understand the evaporation pattern of the implanted K from the evaporation filament, also with the aim to optimize the extraction and implantation voltage. Connected to this, it would be favorable having a better matching standard, i.e., iron with a small but known and homogeneous K concentration. This would help further optimizing the entire extraction procedure and would solve the problem of non-matching standards.

Seventh, it might be possible that Multi-Collector-Inductively-Coupled Plasma (MC-ICP) instruments equipped with a collision cell, that allows removal of Ar, are better instruments in terms of interference-free K measurements (e.g., Télouk et al., 2022). However, for such a set-up, K from the rhenium filament needs to be dissolved, which might add unwanted blank contributions.

Eighth, with the current data set the favored way to calculate cosmogenic ^{40}K/^{41}K ratios is by assuming all ^{39}K to be terrestrial and performing two-component mixing calculations. For some samples (but not for all) plotting the thus calculated $(^{40}K/^{41}K)_{cos}$ ratios as a function of cycle number gives a plateau with constant or almost constant ratios. Using the plateau data gives promising results for some samples. However, this procedure is not the preferred way of interpreting the data because, first, it assumes that all ^{39}K is native K and/or from contamination. This clearly contradicts the major aim of the study to detect clear cosmogenic ^{39}K, ^{40}K, and ^{41}K signals. Second, it assumes that there is a stable fractionation on the filament, i.e., that the fractionation during the entire run is constant and the same as for the standard. An assumption that is not fulfilled for all samples and all cycles.

To summarize, while there are still some open questions, this study presents a major step forward studying cosmogenic K isotope ratios in iron meteorites with the aim to re-establish a consistent and reliable database for ^{40}K-K CRE ages. The currently planned changes and improvements will further enhance the quality of the data.

CRediT authorship contribution statement

H. Khan: Data curation, Investigation, Validation. **I. Leya:** Conceptualization, Data curation, Funding acquisition, Project administration, Resources, Supervision, Visualization, Writing – review & editing. **J. Hoffmann:** Formal analysis, Investigation. **K. Mezger:** Formal analysis, Validation, Writing – original draft.

Declaration of competing interest

The authors declare that they have no known competing financial interests or personal relationships that could have appeared to influence the work reported in this paper.

Acknowledgements

The authors are very grateful to M. Humayun for extremely valuable comments and suggestions for the first draft of this manuscript. We thank Prof. Ozan Unsalan, Faculty of Science, Edge University, Izmir, Turkey, for providing the Kayakent sample. All other samples were from our own collection at the University of Bern. The work was supported by the Swiss National Science Foundation (200020_182447 and 200020_196955).

Appendix 1. Implantation of K into the rhenium filament

During the extraction procedure, the K ions are electrostatically accelerated towards the filament and implanted. With an implantation energy of 4 keV, the SRIM code (Ziegler et al. 2010) calculates an implantation depth of $\sim 32 \times 10^{-10}$ m (=3.2 nm) for a rhenium filament at an incident angle of 0°. However, the depth distribution of implanted ions shows a wide range from almost zero (directly at the surface) to 10 nm. This is also indicated by the ion straggle of $\sim$ 2 nm and a distribution skewness of $\sim$ 2 nm. The recoil losses are $\sim$ 23 %. The implantation depth remains essentially constant for an incident angle up to 20°. However, the percentage of recoiled ions increases with higher incident angles. For example, the recoil losses are $\sim$ 26 % for an incident angle of 20°. Important for the present study is the finding that the implantation depths, including straggle, skewness, and recoil, are essentially the same for ^{39}K, ^{40}K, and ^{41}K. Consequently, large fractionation effects during implantation are not expected.

The ionic radius for K^+ is in the range of 0.133–0.164 nm, depending on coordination. Consequently, most K ions are implanted $\sim$ 20 ionic radii deep into the filament. This implantation depth depends on the energy of the K ions and the incident angle. In addition, the atomic radius for rhenium is $\sim$ 0.137 nm, i.e., the implantation depth also corresponds to 10–20 atomic layers of rhenium. Consequently, the K ions are implanted deeply into the filament with a wide depth distribution, which can account for the difficulties obtaining stable TIMS signals.

Deposition of K in the rhenium filament could reach saturation by implantation. There are $\sim 1.5 \times 10^{13}$ atoms in 1 ng of K. If implantation would only be directly at the surface, saturation would be reached at $\sim 10^{13}$ atoms/mm^2. Optical inspection of the filament after sample extraction indicated an area covered with metal of ca. 2 mm^2. Assuming that this optically modified area corresponds to where K was implanted, 1 ng K would almost but not yet saturate the filament. The saturation limit is further relaxed because the implantation depth is on average $\sim$ 3.2 nm (=3.2×10^{-6} mm), i.e., far deeper than only the immediate surface layer. For example, in a volume of 1 mm × 2 mm × 3.2×10^{-6} mm, i.e., $\sim 6 \times 10^{-6}$ mm^3 there are $\sim 4 \times 10^{14}$ Re atoms, i.e., far more than there are K atoms in the hypothetical 1 ng sample (ρ(Re) = 21.4 g/cm^3, A(Re) = 186 g/mol). Consequently, as long as the amount of K is only a few ng or less, and as long as the implantation area on the filament is not too small, saturation is not expected to be a limiting factor. However, for larger sample amounts and/or narrower focusing, saturation might limit the efficiency of the extraction procedure.

Appendix 2. Evaporation of Fe and condensation onto the filament

Following the approach for the Knudsen effusion cell described by Kendler et al. (2019), the amount of evaporated Fe as a function of temperature and cell dimensions can be calculated via:

$$\frac{dm}{dt} = \frac{P_v A_0 W_0 \sqrt{M}}{\sqrt{2\pi R T}} \quad (1)$$

with P_v the vapor pressure of Fe (Pa = kg / (m s^2)), A_0 the area of the orifice (m^2), and W_0 the dimensionless Clausius factor. The molecular mass of iron is M (kg/mol), R is the general gas constant (J / (mol K)), and T is the temperature in K. The Clausius factor W_0, which characterizes the dimensions of the orifice, is described by the equation:

$$W_0 = \left[1 + \left(\frac{3 l_0}{4 d_0}\right)\right]^{-1} \quad (2)$$

with l_0 as the diameter of the orifice and d_0 the length of the orifice. Equation 1 gives the rate of evaporated iron in kg/s. The crucible set-up used in the experiments is not designed as a Knudsen cell, in which the orifice must be small enough to ensure that the evaporated material undergoes molecular flow. For a molecular flow to establish, atom-wall collisions must dominate over atom–atom collisions. As a first order approximation, the diameter of the orifice must be kept below 1/10 of the mean free path of the vapor species. For a pressure in the 10^{-6} mbar range and a temperature of ca. 1800 K, the mean free path of the evaporated iron atoms is $\sim$ 0.5 m. This gives an upper limit for the orifice of $\sim$ 5 cm. In the present set-up the opening between the crucible and the filament was 1 cm, i.e., small enough. Consequently, the Fe vapor in the low pressure and high temperature environment behaves like an ideal gas, permitting us to use the equation for the Knudsen cell.

For our set-up $A_0 \sim 0.8$ cm^2, $l_0 \sim 1$ cm, $d_0 \sim 1$ mm, the Clausius factor W_0 is $\sim$ 0.12. With a temperature of $\sim$ 1800 K, the mass loss rate of Fe can be calculated as $\sim 6 \times 10^{-4}$ g/s. Assuming an extraction time of $\sim$ 40 min, the total amount of evaporated Fe is $\sim$ 1.5 g, i.e., about half of the sample material evaporates during the extraction procedure. Such a large amount is unexpected but is corroborated by the experimental finding that after sample extraction the weight of the material remaining is substantially lower than the weight of the original sample. Assuming further an area of the filament of $\sim$ 0.1 cm^2 (1 cm length, 0.1 cm width) and homogeneous condensation of the evaporated Fe onto all cold surfaces outside the crucible-aperture assembly, the amount of Fe on the filament would be $\sim$ 200 mg; which is unrealistically high, Such a deposit would be visible on the filament. It is therefore safe to assume that most of the Fe condenses earlier, i.e., on the upper part of the crucible or inside the aperture. Indeed, slight iron condensation was observable in the inside of the aperture. For example, assuming homogeneous condensation of the Fe onto the upper half of the crucible wall and/or inside the aperture, which is $\sim$ 20 cm^2, results in almost all Fe condensing in this area, leaving $\sim$ 10 µg of Fe condensing onto the filament, which is a more reasonable amount. This estimate indicates that there will be some condensation

of Fe onto the filament, likely compromising the ability to obtain stable TIMS signals.

Appendix 3. Details of the extraction system and the extraction procedure

The upper part of the system, which must be ultra clean, comprises the inner part of the metal crucible, the inner crucible, the sample loading system, the filament, and parts of the ion optics. The metal crucible serves as a vacuum barrier between the lower and the upper part of the system. Pumping is via a turbomolecular pump in combination with a three-stage diaphragm pump. Typical pressures are $\sim 10^{-8}$ mbar for a cold system (no heating) and $\sim 10^{-6}$ mbar for a hot system (crucible at $\sim$ 1800 °C). As shown in Fig. 2 in the text, there is an aperture above the crucible with a stepwise drilled opening that helps guiding the positive ions onto the filament and at the same time reduces condensation of other neutral species, including Fe onto the filament. The filament is located above the aperture and is for a regular double-filament set-up used for the TIMS Triton Plus spectrometer. After making the filaments, they were first degassed and then stored for at least a week prior to their use. The distance between the filament and the bottom of the crucible is $\sim$ 80 mm. The filament can easily be changed by removing the top flange. In the current version, the filament can either be heated with a current of $\sim$ 2 A while at ground potential or it can be set to −4000 V with no current flowing (in addition to the degassing after their manufacture, see above). The 2 A that can be used for preheating is far more than typical heating and evaporation currents applied to the filament during TIMS measurements. During the extraction procedure, the K ions are extracted from the iron melt using a strong electric field of $\sim$ 500 V/cm between the sample and the filament, i.e., −4000 V between sample and filament. During extraction, most other volatile elements remain neutral (e.g., Voshage and Hintenberger, 1959,1961) and only a very small part of them reaches the filament; the majority likely condenses onto the much larger cold surfaces of the surrounding. The vacuum inside the system is closely monitored and a pressure lower than 10^{-6} mbar is always maintained. Therefore, the volatiles, including the Fe vapor, are either pumped away or they condense in the colder regions. The outer part of the system is actively cooled by a ventilation system. The crucible is placed in a water-cooled flange and separates the vacuum into upper and lower parts via a gold gasket; all other connections have commercial copper gaskets. After extraction and sample collection, the filament is used for K isotope ratio measurements in a TIMS.

Appendix 4. The development of the extraction system

Version 1: In the first version, the metal crucible was made of tantalum and the liner crucible of graphite. A liner crucible is needed, because at high temperatures, the iron sample would immediately react with the metal crucible forming an alloy, thereby seriously damaging the crucible. Graphite was chosen for several reasons. First, RF heating is known to work very efficiently for graphite (e.g., Patidar et al. 2017) and even though RF heating is dominantly a surface effect, it could be expected that graphite increases the overall heating efficiency. Second, a graphite liner is mechanically stable enough and can therefore serve as a protective layer for the metal crucible. Third, it is anticipated that graphite can be produced very cleanly, i.e., essentially free of K, which is required to reach low blank levels. Fourth, the reaction of the iron with the graphite reduces the melting point, increasing the efficiency of the heating process.

The project started with a careful and thorough testing of the system and by determining the RF-current needed to melt the iron meteorite sample. For the combination tantalum & graphite $\sim$ 190 A is needed for sample melting, which corresponds to $\sim$ 1800 °C (measured using an IR thermometer, not corrected for effects caused by the glass window). During the heating procedure the temperature (RF-current) was slowly increased at a rate of $\sim$ 20 A every 5 min until 120 A was reached. After this, the temperature was increased in steps of $\sim$ 10 A every 5 min until 160 A was reached. The final temperature (RF-current 195 A) was approached at a rate of $\sim$ 5 A every 5 min. This heating procedure permitted a good control of the pressure in the system and avoided much thermal stress on the components. The K extraction was done at 195 A, i.e., slightly above 1800 °C and lasted for 40 min.

While testing the system, some limitations and drawbacks were detected. The most serious problem was with the graphite liner. The iron melt stuck to the graphite liner, producing cracks after just a few heating cycles. Consequently, the molten iron seeped through the cracks, reacted with the tantalum crucible, and corroded it by forming holes. This also affected the outside of the crucible, with the risk of breaking the RF-coil. The problem could not be solved by changing to graphite crucibles from different suppliers. Therefore, parts of the system were re-designed and changed.

Version 2: In the first re-design, the relatively expensive custom-made tantalum crucible was replaced by a similarly reliable molybdenum crucible. Staying with the original dimensions, there was no change for the graphite liner. After this modification, the RF-current required for melting the iron had to be increased from 190 to 245 A. The change in RF current is expected considering that the magnetic permeability and therefore the inductivity of molybdenum is $\sim$ 60 % lower than that of tantalum. In the next step, the distance between the filament and sample was reduced by increasing the bottom of the molybdenum crucible by 20 mm. Doing so, a 20 mm molybdenum cylinder with a diameter fitting the inside of the molybdenum crucible was placed at the bottom of the latter. Consequently, the graphite liner had to be shortened accordingly. This set-up reduced the distance between the filament and the sample from $\sim$ 80 mm to $\sim$ 60 mm. It was anticipated that the stronger electric field promotes K extraction. However, this set-up had a significant drawback as it exacer-

bated the problem of breaking the graphite crucible, because much higher RF-currents were necessary for melting the sample. As a consequence of the higher RF-currents, there was too much thermal stress for some of the relevant components and it was therefore necessary to modify the system and focus on the continuously breaking graphite liner.

Version 3: In the third version of the extraction system, the graphite liner was replaced by a BN (boron nitride) liner, using the original dimensions, i.e., ~80 mm distance between the filament and the bottom of the crucible. BN, which has a high thermal conductivity and is therefore well-suited as a liner material, has been regularly used in our noble gas extraction system with good results (e.g., Ammon et al., 2008a, 2008b, 2011; Smith et al. 2017, 2019; Smith and Leya 2022). The change from graphite to BN as an liner material significantly improved handling and maintaining the system. First, BN is physically stable; it does not stick to the outer molybdenum crucible and can therefore easily be removed for cleaning. Second, the BN liner is easy to clean. The molten and re-crystallized sample can easily be poured out, leaving an almost (despite some minor iron condensation) clean (inner) crucible ready for the next use without any further cleaning step. Consequently, the combination BN liner and molybdenum outer crucible is robust, can be kept clean, and can be used for multiple samples and/or heating cycles. This enables low blanks, which is essential for this project. No adjustment of the extraction temperature was necessary when using the BN inner crucible. Consequently, the anticipated advantage of increasing the RF-heating efficiency by using a graphite crucible was not fulfilled.

In retrospect, this is not surprising considering the so-called *Skin-effect*, which describes the very efficient damping of high frequency currents. Therefore, most of the high-frequency currents are close to the surface. As a numerical example, the penetration depth of RF-currents in the crucible, $\delta_{crucible}$, can be calculated via (e.g., Patidar et al. 2017):

$$\delta_{crucible} = \sqrt{\frac{\rho_{crucible}}{\pi \mu_0 \mu_{crucible} f}}[m] \quad (1)$$

with $\rho_{crucible}$ the resistivity of the crucible (Ω m), which is for molybdenum $\rho_{crucible} = 53$ nΩ m. The magnetic permeability of free space is $\mu_0 = 4\pi \times 10^{-7}$H/m, and $\mu_{crucible}$ is the relative magnetic permeability of molybdenum. For this estimate $\mu_{crucible} = 1$. The frequency of the coil current is given by f (Hz). With a frequency of 300 kHz, which is well within the frequency range of 150–400 kHz of the RF-generator, the penetration depth is less than 1 mm. This is less than the thickness of the wall and the bottom of the crucible. Therefore, the turbulent electric currents, which are responsible for heating, do not reach the inner part of the molybdenum crucible and they are therefore also not reaching the inner crucible, neither for graphite nor for BN. In addition, also the expectation that graphite promotes sample melting by reducing the melting point, did not materialize.

Version 4: Despite the improvements and changes made from version 1 to version 3, the overall performance of the extraction line was still not satisfactory. Extracting enough cosmogenic K from the sample and collecting it on (or in) a filament was still a challenge. All K isotope ratios measured by TIMS were close to the ratios for the terrestrial stan-

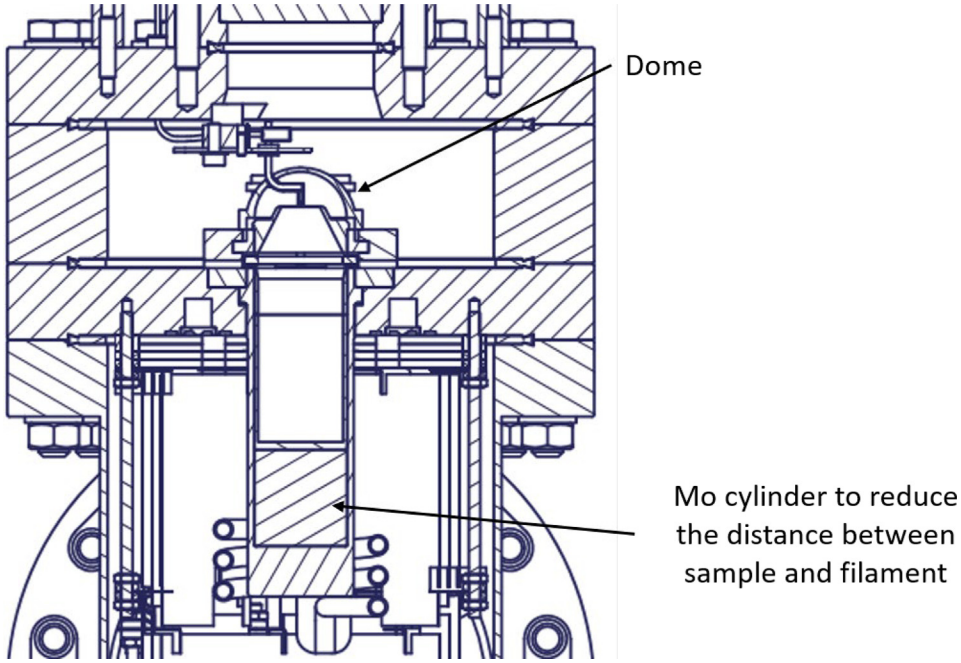

Fig. A4. Engineering drawing of the updated K extraction system (Version 4). The same as Fig. 2, but with the newly installed dome on top of the filament crucible assembly. The dome is expected to increase the efficiency of K extraction from the sample and collection into the filament. For typical dimensions see Fig. 2.

dard thus representing dominantly measurements of either blank or native K both not sufficiently separated from (the wanted) cosmogenic K. With the goal to better guide the electric field into the crucible and thereby promoting extraction and collection of K, a spherical cover located above the entire filament-crucible assembly was designed and constructed.

Figure A4 shows an engineering drawing of the updated system, i.e., it shows the (half) spherical cover made of stainless steel placed over the filament. The motivation for this change was to increase the electric field strength between the filament and the sample, thereby promoting K extraction out of the sample.

References

Alexeev, V.A., 2016. Long-term galactic cosmic ray variations over the last billion years based on cosmic-ray exposure ages of iron meteorites. Geochem. Intern. 54, 78–84.

Amelin, Y., Merle, R., 2021. Isotopic analysis of potassium by total evaporation and incipient emission thermal ionization mass spectrometry. Chem. Geol. 559119976.

Ammon, K., Masarik, J., Leya, I., 2008a. Noble gases in Grant and Carbo and the influence of S- and P-rich mineral inclusions on the 41K–40K dating system. Meteorit. Planet. Sci. 43, 685–699.

Ammon, K., Leya, I., Lavielle, B., Gilabert, E., David, J.-C., Herpers, U., Michel, R., 2008b. Cross sections for the production of helium, neon, and argon isotopes by proton-induced reactions on iron and nickel. Nucl. Inst. Methods Phys. Res. B 266, 2–12.

Ammon, K., Leya, I., Lin, Y., 2011. Noble gases in the Xinjiang (Armanty) iron meteorite – A big object with a short cosmic-ray exposure age. Meteorit. Planet. Sci. 46, 785–792.

Aylmer, D., Bonanno, V., Herzog, G.F., Weber, H., Klein, J., Middleton, R., 1988. ^{26}Al and ^{10}Be production in iron meteorites. Earth Planet. Sci. Lett. 88, 107–118.

Birck, J.L., Allegre, C., 1983. Systematics of spallation products in Iron meteorites. Meteoritics 18, 267.

Birck J. L., Allegre C. 1985. Isotopes produced by galactic cosmic rays in iron meteorites. In: CNES Isotopic Ratios in the Solar System: 21-25 (SEE N86-33216-88).

Buchwald, V.F., 1977. The mineralogy of iron meteorites. Philos. Trans. R. Soc. Lond.**A** 268, 453–491.

Coath, C.D., Steele, R.C.J., Lunnon, W.F., 2013. Statistical bias in isotope ratios. J. Anal. at. Spectrom. 28, 52–58.

Dauphas, N., Schauble, E.A., 2016. Annu. Rev. Earth Planet. Sci. 44, 709–783.

Gies, D.R., Helsel, J.W., 2005. Ice age epochs and Sun's path through the galaxy. Astrophys. J. 626, 1833–1841.

Hampel, W., Schaeffer, O.A., 1979. ^{26}Al in iron meteorites and the constancy of cosmic ray intensity in the past. Earth Planet. Sci. Lett. 42, 348–358.

Imamura, M., Shima, M., Honda, M., 1980. Radial distribution of spallogenic K, Ca, Ti, V, Mn isotopes in iron meteorites. Z. Naturforsch. 35a, 267–279.

Jahnke, K., 2005. On periodic clustering of cosmic ray exposure ages of iron meteorites. A & A No. 4155J.

Kendler, R., Dreisbach, F., Seif, R., Pollak, S., Petermann, M., 2019. Measuring low vapor pressures employing the Knudsen effusion technique and a magnetic suspension balance. Rev. Sci. Instrum. 90. https://doi.org/10.1063/1.5091606.

Khan, H.M., 2022. Cosmogenic Potassium in Iron Meteorites. University of Bern, p. 78, PhD thesis.

Kossert, K., Günther, E., 2004. LSC measurement of the half-life of ^{40}K. Appl. Radiat. Isot. 60, 459–464.

Lavielle, B., Marti, K., Jeannot, J.P., Nishiizumi, K., Caffee, M., 1999. The ^{36}Cl-^{36}Ar-^{40}K-^{41}K records and cosmic ray production rates in iron meteorites. Earth Planet. Sci. Lett. 170, 93–104.

Naumenko, M.O., Mezger, K., Nägler, T.F., Villa, I.M., 2013. High precision determination of the terrestrial ^{40}K abundance. Geochim. Cosmochim. Acta 122, 353–362.

Ogliore, R.C., Huss, G.R., Nagashima, K., 2011. Ratio estimation in SIMS analysis. Nuclear Instruments and Methods in Physics Reseaerch B 269, 1910–1918.

Patidar, B., Hussain, M.M., Jha, S.K., Sharma, A., Tiwari, A.P., 2017. Analytical, numerical and experimental analysis of induction heating of graphite crucible for melting of non-magnetic materials. IET Electr. Power Appl. 11, 342–351.

Rahmstorf, S., Archer, D., Ebel, D., Eugster, O., Jouzel, J., Maraun, D., Neu, U., Schmid, G., Severinghaus, J., Weaver, A.J., Zachos, J., 2004. Cosmic rays, carbon dioxide, and climate. Eos 85, 1739–1746.

Scherer, K., Fichtner, H., Borrmann, T., Beer, J., Desorgher, L., Flückiger, E., Fahr, H.J., Ferreira, S.E.S., Langner, U.W., Potgieter, M.S., Heber, B., Masarik, J., Shaviv, N.J., Veizer, J., 2006. Interstellar-terrestrial relations: Variable cosmic environments, the dynamic heliosphere, and their imprints on terrestrial archives and climate. Space Sci. Rev. 127, 327–465.

Shankar, N., 2011. Cosmic Ray Exposure Ages of Iron Meteorites Using 39K–40K-41K Dating. Graduate-School-New Brunswick Rutgers, The State University of New Jersey, p. 290, PhD thesis.

Shaviv, N.J., 2002. Cosmic ray diffusion from the galactic spiral arms, iron meteorites, and a possible climate connection. Phys. Rev. Lett. 89, id. 051102.

Shaviv, N.J., 2003. The spiral structure of the Milky Way, cosmic rays, and ice age epochs on earth. New Astron. 8, 39–77.

Shaviv N. J., Veizer J. 2003. Celestial driver of Phanerozoic climate, EGS – AGU – EUG Joint Assembly. #13041.

Sloan, T., Wolfendale, A.W., 2013. Cosmic rays and climate change in the past 1000 million years. New Astron. 25, 45–49.

Smith, Th., Cook, D.L., Merchel, S., Pavetich, S., Rugel, G., Scharf, A., Leya, I., 2019. The constancy of galactic cosmic rays as recorded by cosmogenic nuclides in iron meteorites. Meteorit. Planet. Sci. 54, 2951–2976.

Smith, Th, Leya, I., 2022. The noble gas inventory in metal samples and troilite inclusions from IIIAB iron meteorites: Reinvestigating the live 129I–129X dating method. Meteorit. Planet. Sci. 57, 1421–1440.

Smith, Th, Hofmann, B.A., Leya, I., Merchel, S., Pavetich, S., Rugel, G., Scharf, A., 2017. The cosmic exposure history of the Twannberg iron meteorite (IIG). Meteorit. Planet. Sci. 52, 2241–2257.

Télouk, P., Albalat, E., Tacail, T., Arnaud-Godet, F., Balter, V., 2022. Steady analysis of potassium stable isotopes using a Thermo Scientific Neoma MC-ICP-MS. J. Anal. at. Spectrom. 37, 1259–1264.

Voshage, H., 1967. Bestrahlungsalter und Herkunft der Eisenmeteorite. Z. Naturforsch. 22a, 477–506.

Voshage, H., 1978. Investigations on cosmic-ray produced nuclides in iron meteorites, 2. New results on ^{41}K/^{40}K-^{4}He/^{21}Ne exposure ages and the interpretation of age distributions. Earth Planet. Sci. Lett. 40, 83–90.

Voshage, H., 1984. Investigation of cosmic-ray produced nuclides in iron meteorites VI - The Signer-Nier model and the history of the cosmic radiation. Earth Planet. Sci. Lett. 71, 181–194.

Voshage, H., Feldmann, H., 1979. Investigation on cosmic-ray produced nuclides in iron meteorites. 3. Exposure ages, meteoroid sizes, and sample depths determined by mass spectrometric analysis of K and rare gases. Earth Planet. Sci. Lett. 45, 93–108.

Voshage, H., Feldmann, H., Braun, O., 1983. Investigations of Cosmic-Ray Produced Nuclides in Iron Meteorites: 5. More Data on the Nuclides of K and Noble Gases, on Exposures Ages and Meteoroid Sizes. Z. Naturforsch. 38a, 273–280.

Voshage, H., Hintenberger, H., 1959. Kalium als Reaktionsprodukt der kosmischen Strahlung in Eisenmeteoriten. Z. Naturforsch.**A** 14, 828–838.

Voshage, H., Hintenberger, H., 1961. Massenspektrometrische Isotopenhäufigkeitsmessungen an Kalium aus Eisenmeteoriten und das

Problem der Bestimmung der 41K–40K Strahlungsalter. Z. Naturforsch. 16, 1042–1053.
Wallmann, K., 2004. Impact of atmospheric CO_2 and galactic cosmic radiation on Phanerozoic climate change and the marine $\delta^{18}O$ record. Gechemistry, Geophysics, Geosystems 5, Q06004.
Weber, H.W., Braun, O., Begemann, F., 1986. Helium, Neon, and Argon in the Iron Meteorites Dongling, Nantan and Ningbo. Geochemistry 5, 320–330.
Wieler, R., Beer, J., Leya, I., 2013. The galactic cosmic ray intensity over the past 106–109 years as recorded by cosmogenic nuclides in meteorites and terrestrial samples. Space Sci. Rev. 176, 351–363.
Ziegler, J.F., Ziegler, M.D., Biersack, J.P., 2010. SRIM – The stopping and range of ions in matter (2010). Nucl. Inst. Methods Phys. Res. B 268, 1818–1823.